Linear and Nonlinear Analysis of a Clamped Plate Subjected to Air-Blast Loading

By

Yang Liu

A Thesis

Submitted to the Faculty of Graduate Studies

In Partial Fulfillment of the Requirements

For the Degree of

MASTER OF SCIENCE

Department of Civil Engineering
University of Manitoba
Winnipeg, Manitoba, Canada

Thesis Advisor: Assistant Professor N. Rattanawangcharoen, Ph.D., P.Eng.

THE UNIVERSITY OF MANITOBA

FACULTY OF GRADUATE STUDIES

*****

COPYRIGHT PERMISSION

Linear and Nonlinear Analysis of a Clamped Plate Subjected to Air-Blast Loading

by

Yang Liu

A Thesis/Practicum submitted to the Faculty of Graduate Studies of The University of Manitoba in partial fulfillment of the requirement of the degree

of

Master of Science

Abstract

This study presents an elastic linear and nonlinear analysis of a fully clamped thin plate subjected to air-blast loading. The dynamic equations of motion for the plate are derived based on the classical thin plate theory and the von Kármán geometric nonlinear theory. The geometry and the loading of the problem considered is symmetric about the mid-point of the plate and, therefore, the four-mode displacement function is assumed. The Galerkin method is used to formulate a set of four differential equations of motion for both linear and nonlinear analysis. The Friedlander distribution is modified to incorporate the dynamic interactions between the blast wave front and the plate's surface. The numerical integration of the blast load over the area of a small element of the plate is carried out by the Gaussian quadrature. The linear and nonlinear equations of motion are solved numerically using the fourth-order Runge-Kutta method. The displacement time-histories of the plates subjected to the blast load obtained by the proposed model agree well with the existing experimental and finite-element analysis results. The numerical investigation of the dynamic interactions between the wave front and the plate's surface shows that the peak pressure calculated from the modified Friedlander model depends on the radial distance-to-plate's dimension ratio but the maximum impulse does not. Since the acceleration response of the plate subjected to blast load depends on the peak pressure, this modified Friedlander model should be used in the analysis for all radial distance-to-plate's dimension ratio. On the other hand, if the displacement response of the plate is of interest, the Friedlander model may be used because the

displacement response of the plate depends only on the maximum impulse. The effect that the plate's aspect ratio, the plate's surface area, and the charge location has on the response of the plate subjected to air blast loadings is also studied. It is found that a square plate is the weakest configuration among all of the rectangular shapes. For a square plate, the flexibility of the plate increases when the plate's area increases. However, when the plate's dimension is larger than 900 mm × 900 mm in linear analysis or 1000 mm × 1000 mm in nonlinear analysis, the flexibility of the plate decreases for the loading considered. The charge location does not have significant effect on the maximum displacement of the plate.

Acknowledgment

I would like to express my sincere appreciation and gratitude to my advisor, Dr. Nipon Rattanawangcharoen, for his guidance for the past two years, and for proposing the topic of this thesis. His constant encouragement and advice have been invaluable to me during the course of this research. Without his support, this work would not have been possible. I would also like to thank Dr. Arvind Shah and Dr. Gary Wang for being in the committee. Financial support from the NSERC is greatly appreciated.

I would also like to acknowledge Mohammad M. Hoque, Nibong Ungkurapinan, Cameron Ward, and Lena Tanaka for their assistance.

TABLE OF CONTENTS

LIST OF TABLES

LIST OF FIGURES

LIST OF SYMBOLS

A	=	area of the target
a	=	plate length
b	=	plate width
C_p	=	constant pressure
C_v	=	constant volume
c_s	=	local speed of sound
c_w	=	shock front velocity
D	=	bending rigidity
dx	=	rectangular element of thin plate of length
dy	=	rectangular element of thin plate of width
E	=	modulus of elasticity
F	=	stress function
h	=	plate thickness
I	=	blast impulse
k	=	heat capacity ratio
k_1	=	parameter in RK4's formulas
k_2	=	parameter in RK4's formulas
k_3	=	parameter in RK4's formulas
k_4	=	parameter in RK4's formulas
M	=	Mach number

M_1 = parameter in RK4's formulas

M_2 = parameter in RK4's formulas

M_3 = parameter in RK4's formulas

M_4 = parameter in RK4's formulas

M_r = reflected Mach number

M_x = incident Mach number

M's = moment

N's = normal forces

p_a = atmospheric pressure

p_r = reflected wave pressure

p^o = peal overpressure

$p(t)$ = instantaneous overpressure at time t

$p(x,y)$ = transverse distributed load

$p(x,y,t)$ = instantaneous distributed overpressure at time t

Q's = transverse shear force

R = radial distance

t = time

t_a = arrival time

t_d = positive phase duration

v_0 = initial condition in RK4's formulas

W = explosion charge mass

w = transverse displacement

X_1	=	continuous function in RK4's formulas
X_1'	=	First-order differential equation
X_2	=	First-order differential equation
X_2'	=	Second-order differential equation
y	=	continuous function in RK4's formulas
$\dot{y}$	=	First-order differential equation
$\ddot{y}$	=	Second-order differential equation
y_0	=	initial condition in RK4's formulas
Z	=	scaled distance
Δt	=	size of the interval
Λ	=	reflection coefficient
α	=	decay coefficient
β	=	angle of incidence
δ	=	reflection angle
ξ	=	damping ratio
μ	=	damping coefficient of the plate
ν	=	Poisson's ratio
ρ	=	mass density of the plate
ω	=	natural frequency
∇^4	=	biharmonic (or bilaplacian) operator

Chapter I

Introduction

1.1 General

Thin plates are used in naval ships, aircrafts, and various industrial structures. These structures could be subjected to air-blast and shock loads. The knowledge and understanding of the response of thin plates under blast loading are important. Hence, the study of thin plates subjected to explosive loads has received a considerable attention during the last decade.

Explosion is a type of reaction caused by physical and chemical changes. When explosive matter is detonated, massive energy is released causing a violent expansion of hot gases originating a pressure wave moving outward at a very high velocity from its source. This high velocity pressure wave travels to an observation point forming an extremely high pressure front followed by a quasi exponential decay back to the ambient pressure and a negative pressure where the pressure is less than the ambient pressure. When the shock wave hits a target's surface, the wave reflects with generally higher pressure depending on the peak pressure of the incident wave, the angle at which it strikes the surface, the temperature of the ambient, the surrounding ambient, the surrounding wind velocity and direction, and the nature of the surface. This reflected overpressure wave is superimposed on the static overpressure a loading applying to the surface of the target (Lam et al. 2004). Unless the surface area of the

target is considerably small in comparison to the stand-off point for a given charge, the air-blast wave front will not impinge all the position on the surface at the same time.

1.2 Literature review

The study of a response of a structure to air-blast loading is very important in the design and the assessment of vulnerability of the structure. The dynamic response of thin plates to air-blast loading has been studied for many years. The following literature review summarizes the works on the response of thin plates to blast loading by a) experiments, b) numerical simulations, and c) analytical analysis, respectively.

Houlston et al. (1985) and Houlston and slater (1987) performed several experiments on clamped metal plates and stiffened plates subjected air-blast loading and underwater shock loads. The plates used in the experiment were 508 mm × 508 mm with the thickness of either 3.4 mm or 1.5 mm. The stand-offs of the charge varied from 200 cm to 305 cm. They presented measured pressure time histories of the loadings, strain time histories, displacement time histories, velocity time histories, and acceleration time histories of the experiments. The experimental results provided a good understanding of the response of metal plates to blast loading. Jacinto et al. (2001) and Ambrosini and Jacinto (2005) presented their experimental works on an all edge-clamped and a cantilevered rectangular metal plates. The plate dimensions in their experiments were 1.0 m ×1.5 m × 2.1 mm for the cantilevered plate and 0.95 m × 0.95 m × 0.9 mm for the all edge-clamped plate. The stand-offs of the charge varied

from 30 m to 60 m. Pressure time histories and acceleration time histories were recorded and presented. Türkmen (2002) presented experimental strain time histories of clamped laminated cylindrical panels subjected air-blast load. The panel dimensions were 180 mm × 180 mm with thicknesses of 1.2 and 1.4 mm. The stand-off was 1000 mm. Chung and Nurick (2005) reported their experiments on quadrangular stiffened and unstiffened clamped plates subjected to a uniform blast load. The dimensions of the hot rolled mild steel plates used were 126 mm × 126 mm × 12 mm. The impulse of the blast load was high enough to produce large inelastic deformation. Veldman et al. (2006) studied the effects of pre-pressurization clamped aluminum plates subjected to blast load. The plate dimensions were 152 mm × 152 mm × 1.6 mm where the charges were 0.91m and 1.52 m away. The negative static pressure was applied to the internal face of the plates before the blast load was applied. Strain time histories of the plate were presented. They found that the increase in the peak blast induced strain due to pre-pressurization was insignificant.

Numerical analysis of plates and shells subjected to blast loads has been presented during the past two decades. Houlston et al. (1985) used the finite element software ADINA to analyze plates subjected to air-blast loading for an elastic response. The results of the numerical analysis showed a good agreement with their experimental results. Later on, Houlston and Desrochers (1987) did a nonlinear analysis using ADINA to investigate the dynamic response of panels subjected to air-blast loading. In their study, several boundary conditions were considered. Recently, Jacinto et al. (2001) and Ambrosini (2005) used commercial software ABAQUS and COSMOS to

analyze unstiffened steel plates with different boundary conditions subjected to air-blast loading, and the result showed a very good correlation with the prediction of the experimental results. Apart from metal plates, Mosalam and Mosallam (2001) used DIANA 7.2 to perform numerical finite element analysis of reinforced concrete slabs both as-built and retrofitted with carbon fibre reinforced polymer strips subjected to a blast load.

Only a few theoretical studies investigated the response of plates subjected to a blast load. Teng et al. (1996) proposed a one-mode response of simply supported and fixed supported square thin plates under air-blast loading. The loading was assumed to distribute uniformly over the plate surfaces. The plate considered has dimensions of 508 mm × 508 mm × 3.4 mm. Turkmen (2002) investigated the dynamic behavior of clamped laminated composite cylindrical shells subjected to air-blast loading. He derived the governing equations of motion based on the Love's theory of thin shell assumption. The uniformly distributed Friedlander model was used as a loading. Nine-term assumed displacement was employed. The strain-time history results were compared with the experimental and finite element results from ANSYS.

On the theoretical analysis of thin plates subjected to harmonic loads, several researchers employed two-mode model in their studies. Abe, Kobayaski and Yamada (1998) employed a two-mode analysis to find the response of a simply supported rectangular laminated plate subjected to a harmonic excitation. Shu, Han, and Yang (1999) used a two-mode model to analyze the chaotic motion of a large deflection plate. In research by Lai, chen and Yeh (2002), the two-mode model approach

predicted the chaotic and bifurcation dynamics for a simply supported rectangular plate. For linear elastic plates subjected to general dynamic loading, Chia (1980) presented linear analysis of plates subjected to general loadings. Taylor and Govindjee (2004) used the classical double cosine series expansion and the Sherman-Morrison-Woodbury formula to solve clamped rectangular plates subjected to general dynamic loadings.

Woznica et al. (2001) studied the effects of temperature on the response of the plate. They found that the temperature effect was very important in the response of metallic plates subjected to explosion. The dynamic response of square plates and stiffened plates subjected to a uniform blast loading and a localized blast loading were obtained experimentally and numerically by Chung et al. (2005) and Langdan et al. (2005). In their studies, the temperature-dependent material properties were used to analyze. Xue and Hutchinson (2003) investigated the dynamic response of sandwich plate subjected to air-blast loading. It was shown that the sandwich plate with sufficiently strong cores had more resistance to blast load than solid plates of the same material and weight on subjected to large air-blast loading. The dynamic response of elastic-plastic plates was obtained experimentally, numerically, and simplified analytically by Cichocki and Perego (1997). Veldman et al. (2006) investigated the effects of pre-pressurization on the response of clamped plates to blast loads and concluded that pre-pressurization had very little effect on the blast response of clamped plates.

1.3 Objective & Scope

From the literature review, it can be seen that all the works related to plates subjected to air-blast loads have been carried out either experimentally, numerically, or theoretically assuming the blast wave front arrives every point of the target's surface at the same time. To the best of the author's knowledge, there is no investigation of a response of plates to a blast load considering dynamic interactions of the blast wave front with the plate surface. The objectives of this research work are, therefore

- To modify the Friedlander model of a blast load distribute to incorporate dynamic interactions of the blast wave front with the plate surface,
- To investigate the effect the dynamic interactions of the blast wave front with the plate surface has on the linear and nonlinear behaviors of the plate subjected to blast load, and
- To study the effect of the plate's aspect ratio, the plate's area, and the charge location on the response of a plate subjected to air-blast load.

In the study, the governing equations will be solved numerically using the fourth order Runge-Kutta technique. The study considers only elastic deformation of the plate and the plate is made of isotropic materials. Non-stiffened plate is considered. Effects of temperature are neglected and pre-pressurization are not considered. The blast loading is assumed to be symmetric with respect to the middle point of the plate.

1.4 Thesis Organization

General concepts on blast load will be briefed in Chapter II. Basics of the classical

thin plate theory, the von Kármán geometric nonlinear theory, and the Fourth-order Runge-kutta technique will be provided in Chapter III. The formulation of the equations of motion and their solutions will be presented in Chapter IV. The modified Friedlander model will also be included in Chapter IV. Numerical results will be discussed in Chapter V. The conclusion of this study and the recommendation on the future study will be provided in Chapter VI.

Chapter II

Blast Loading

2.1 Introduction

The phenomenon resulting from a rapid release of energy is called an explosion. This energy may come from an explosive such as gunpowder, wheat flour dust in a grain elevator, pressurized steam in a boiler, or an uncontrolled nuclear transformation (Kinney and Graham, 1985). Some of the terminologies and the basic background on the subject of blast will be presented in this chapter.

2.2 Detonation

When the explosive substance is oxidized in some way, a large amount of energy is released to the atmosphere and this phenomenon is called detonation. Smith and Hetherington (1994) gave a basic schematic of the detonation process in a spherical change. As show in Figure 2.1, at the point of initiation of the detonator, chemical bonds of the explosive matter are broken. This break of the chemical bonds creates an enormous exothermic reaction which compresses the surrounding substances causing a high velocity shock wave. The velocity of the shock wave is multiplied as the reaction energy increases in density, temperature, and pressure behind it. The shock wave will move away from the point of initiation. The shock wave front is constantly reinforced by the reaction energy from material just in front of it until it reaches the

free air boundary. The physics related to the formation of the detonation wave and its velocity was described by Zukas and Walters (1997).

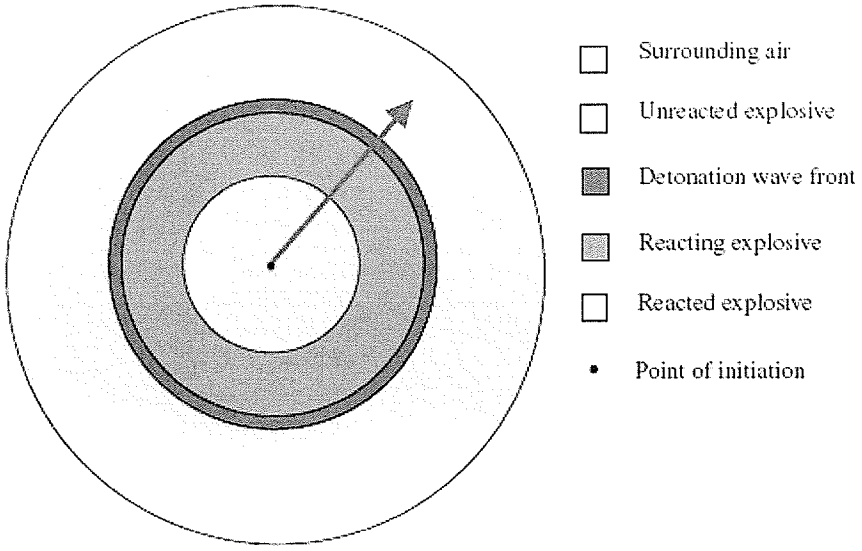

Figure 2.1 Detonation mechanisms within the explosive (source: Smith and Hetherington, 1994)

2.3 Blast Waves

When the surrounding air of the explosion is suddenly pushed back with great force, a blast wave is produced. In Figure 2.2, Kinney and Graham (1985) showed the pressure pulse of an arbitrarily chosen initial configuration in order to illustrate the formation of a blast wave. Each individual part of the pulse propagates outward at the speed of sound particular to the medium it passes through. The higher pressure parts move faster and hence produce higher temperature. The front of the blast wave generates the shock discontinuity.

In Figure 2.3, as the wave expands, the blast energy increasingly absorbed by the

surrounding air retards the wave speed. This further reduces air density and pressure at the wave head. The radiating waves increase in volume, causing explosive gas to expand and pressure to be reduced behind the front, as well.

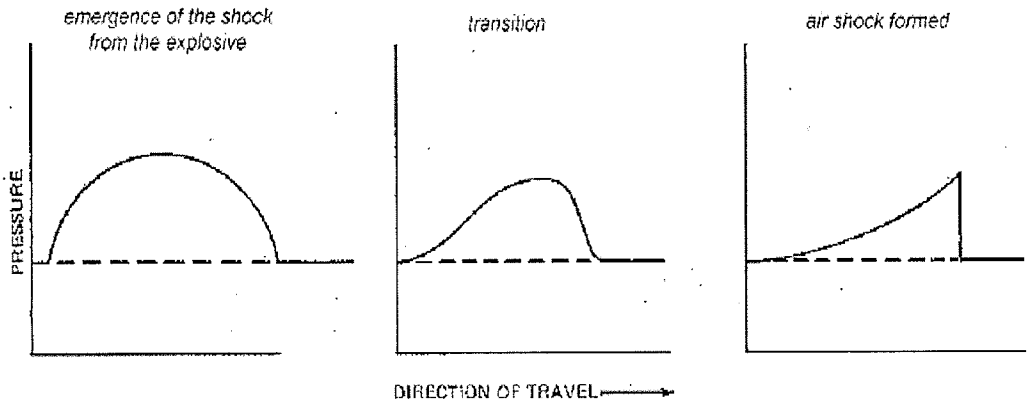

Figure 2.2 Illustrating the development of explosive shock (source: Kinney and Graham, 1985)

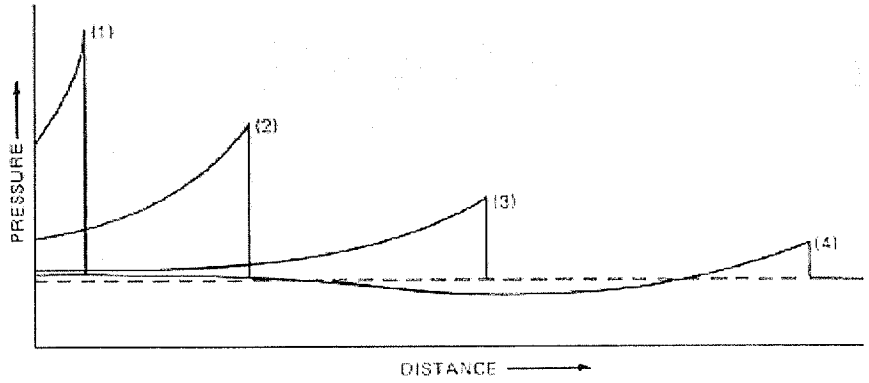

Figure 2.3 A distribution of pressure observed along a base line, at regular time intervals, as blast wave moves through air medium (source: Kinney and Graham, 1985)

The speed of sound must be considered in investigations of blast and shock. For convenience in calculation, a dimensionless index called *Mach number*, M , is used. Mach number is defined as a ratio of the magnitude of a velocity to the local speed of

sound and may be written as

$$M = \frac{c_w}{c_s} \tag{2.1}$$

where M is the Mach number ,

c_w is a shock front velocity, and

c_s is a local speed of sound.

Figure 2.4 shows a typical pressure-time history of blast loading. At an arrival time of t_a after the explosion, the far-location pressure abruptly leaps to peak overpressure. Any object located here suffers an immediate lateral force that is equivalent to the overpressure times the expected area of the radial line of the blast wave. However, this situation does not remain static, because the overpressure dissipates, according to a pressure-time formula. In ideal gas conditions, the positive portion of the blast pressure-time history can be approximated by a Friedlander model as:

$$p(t) = p^o(1 - \frac{t - t_a}{t_d})e^{-\alpha\frac{t-t_a}{t_d}} \tag{2.2}$$

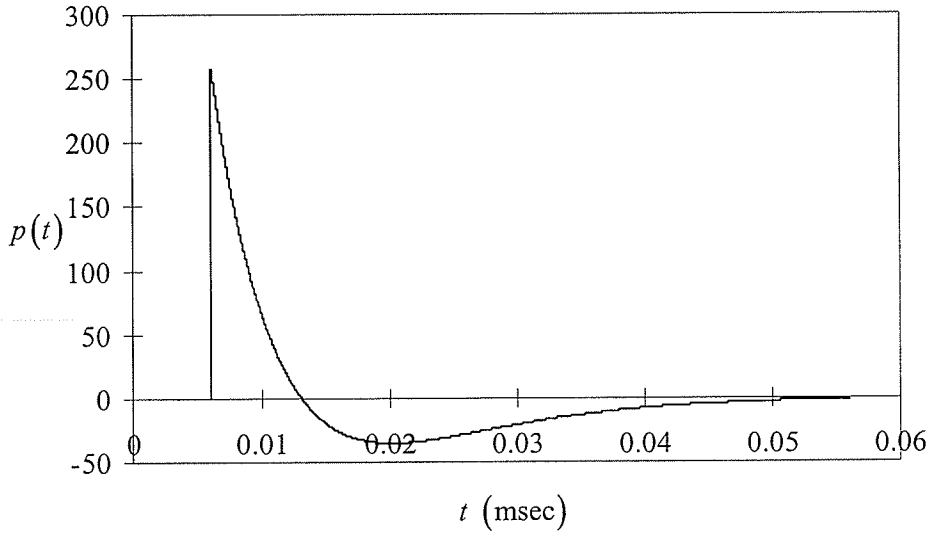

Figure 2.4 Typical curves for a blast wave

where $p(t)$ is an instantaneous overpressure at time t,

p^o is the peak overpressure,

t_a is the arrival time,

t_d is the positive phase duration, and

α is a decay coefficient.

The surrounding atmosphere will return to its original state after the explosion. Over-expansion generates the pressure which is under the atmospheric level, negative pressure. It is called *under-pressure.* The under-pressure should not be higher than one atmosphere.

2.4 Near and Far Field Blasts

Depending on a distance between the detonation point and a target, and target's dimensions, a blast loading on the target may be considered as a *near field* or a *far field loading.* The difference between a near field and a far field blast loading is the curvature of the blast front as it interacts with the target.

Near field loading is defined by $Z \ll 1$ (Lam et al., 2004) where Z is a scaled distance and is expressed as

$$Z = \frac{R}{W^{1/3}} \tag{2.3}$$

where R is a radial distance,

W is an explosion charge mass.

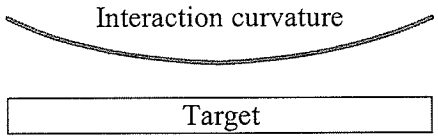

Figure 2.5: Blast curvature for near field blasts

Near field loading is shown in Figure 2.5. The high interaction curvature means that the loading is a spatially-varying transient loading. This type of loading may occur when a small target is in close proximity of the detonation point or when the target is relatively large.

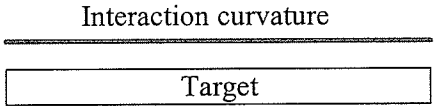

Figure 2.6 A blast curvature for a far field blast

Figure 2.6 shows a typical far field blast loading. This type of loading may be produced by a small charge mass on a relatively small target at a near radial distance or by a large charge mass at a large radial distance on a small target. Because the far field loading has enough time for the blast wave front to arrive every point on the target's surface at the same time, the loading on the target has a low interaction curvature.

2.5 Reflected Shock

The gas expansion stops when the initial blast wave impinges on the relatively rigid target surface. The blast wave is reflected back into the incident medium with an increase in the pressure. Reflected pressure may be expressed as

$$p_r = \Lambda p^o \tag{2.4}$$

where p_r is a reflected wave peak pressure, and

Λ is a reflection coefficient depending on the direction of the reflection.

Reflection has there types: (1) Normal reflection; (2) Oblique reflection; and (3) Mach stem formation.

2.5.1 Normal Reflection

Normal reflection occurs when the blast wave impinges on the relatively rigid surface and the blast wave front is parallel to this surface, as shown Figure 2.7. The reflection coefficient depends on the Mach number and is often expressed as a function of the incident Mach number M_x as

$$\Lambda = \frac{(3k-1)M_x^2 + (3-k)}{(k-1)M_x^2 + 2} \tag{2.5}$$

where k is heat capacity ratio and

$$k = \frac{C_P}{C_V} \tag{2.6}$$

C_P is a constant pressure, and

C_V is a constant volume.

If the explosive is in an ideal atmospheric surrounding, k is equal to 1.4. The normal reflection coefficient, Eqn. (2.5), changes to

$$\Lambda = \frac{8M_x^2 + 4}{M_x^2 + 5} \tag{2.7}$$

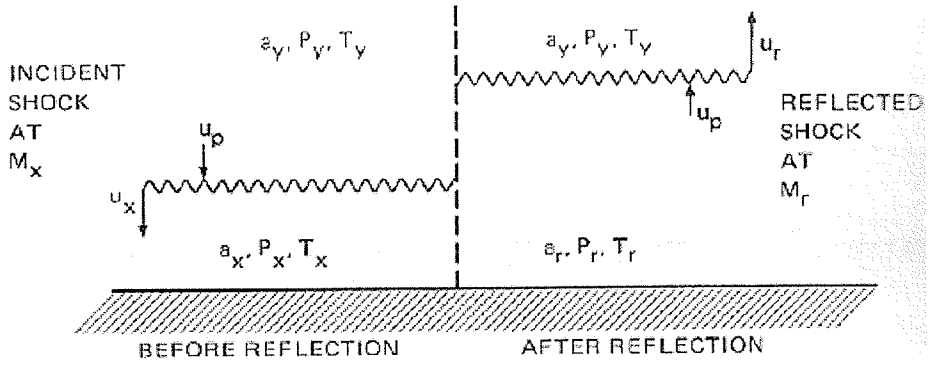

Figure 2.7 A normal reflection (source: Kinney and Graham, 1985)

2.5.2 Oblique Reflection

Oblique reflection occurs when the blast wave impinges on the surface at a small angle between the blast wave front and surface. Figure 2.8 illustrates that for the angle of incidence β and the initial shock M_x, the resulting reflected shock M_r, is at the angle of reflection δ. The reflection angle δ depends on the Mach number M_x and other thermodynamic properties.

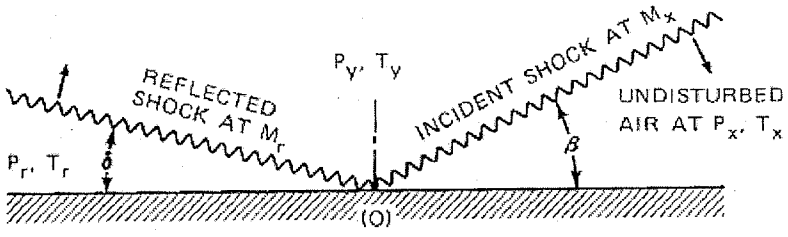

Figure 2.8 An oblique reflection (source: Kinney and Graham, 1985)

The relation between angle of incidence and angle of reflection for shock waves are shown in Figure 2.9. In the figure, incident Mach number M_x runs from one, a sound wave, to five or a strong shock wave. Reflected Mach number M_r for a specific angle of incidence and a specific incident Mach number M_x can be obtained

from Figure 2.10. The reflection coefficient for oblique reflection can be obtained by

$$\Lambda = \frac{\left(7M_r^2 - 1\right)\left(7M_x^2 - 1\right) - 36}{42\left(M_x^2 - 1\right)} \tag{2.8}$$

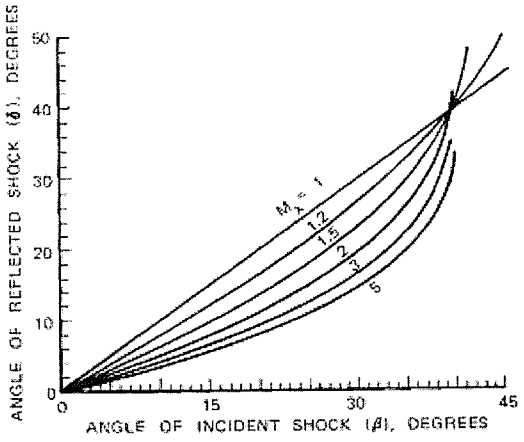

Figure 2.9 Angle of reflected shock vs. angle of incident shock (source: Kinney and Graham, 1985)

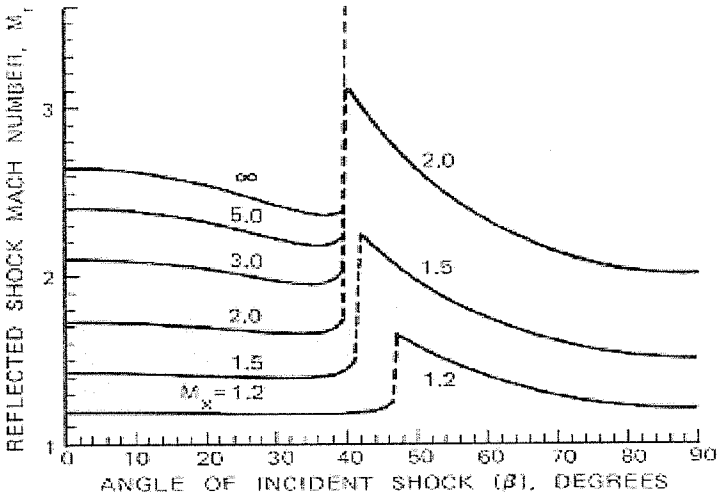

Figure 2.10 Reflected shock Mach number vs. angle of incident shock (source: Kinney and Graham, 1985)

2.5.3 The Mach Stem Formation

Mach stem formation is a spurt-like effect that happens when a shock front strikes a

surface at an angle close to what is called a grazing incidence shown in Figure 2.11. A grazing incidence means that the incident angle is equal to 90 degrees.

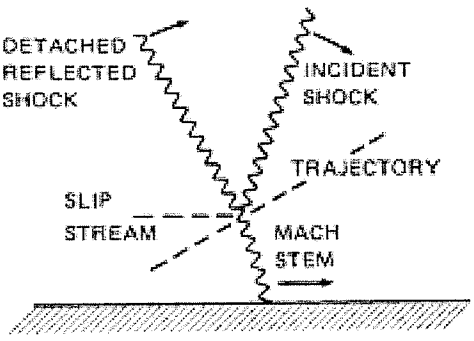

Figure 2.11 The Mach stem formation (source: Kinney and Graham, 1985)

A Mach stem augments the overpressure on the outside of an object. This can be explained using a reflection coefficient Λ, the ratio of the overpressure to the incident angle of the shock. Figure 2.12 plots the reflection coefficients associated with the shock Mach number M_x and the incident shock angle β.

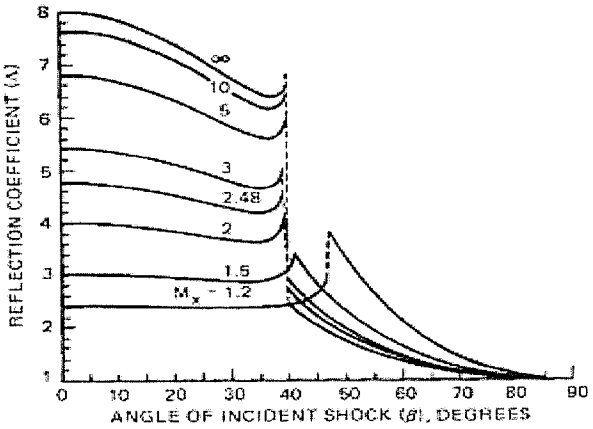

Figure 2.12 Reflection coefficient associated with angle of incident shock (source: Kinney and Graham, 1985)

2.6 Numerical Analysis of Blast Loading

Bode-type equations which calculate blast loading were formed by Kinney and

Graham (1985). The overpressure p^o can be evaluated from the scaled distance by the following equation:

$$\frac{p^o}{p_a} = \frac{808\left[1+\left(\frac{Z}{4.5}\right)^2\right]}{\sqrt{1+\left(\frac{Z}{0.048}\right)^2}\sqrt{1+\left(\frac{Z}{0.32}\right)^2}\sqrt{1+\left(\frac{Z}{1.35}\right)^2}} \tag{2.9}$$

where p_a is an atmospheric pressure.

The arrival time of the shock wave to the target at a radial distance R away from the charge can be mathematically expressed by

$$t_a = \left(\frac{1}{c_s}\right)\int_{r_c}^{R}\left(\frac{1}{M_x}\right)dr \tag{2.10}$$

where r_c is the radius of the charge.

The duration of the positive pressure phase can be evaluated by

$$\frac{t_d}{W^{1/3}} = \frac{980\left[1+\left(\frac{Z}{0.54}\right)^{10}\right]}{\left[1+\left(\frac{Z}{0.02}\right)^3\right]\left[1+\left(\frac{Z}{0.74}\right)^6\right]\sqrt{1+\left(\frac{Z}{6.9}\right)^2}} \tag{2.11}$$

The blast impulse per unit area equation is

$$\frac{I}{A} = \frac{0.067\sqrt[2]{1+(Z/0.23)^4}}{Z^2\sqrt[3]{1+(Z/1.55)^3}} \tag{2.12}$$

Here I is the blast impulse and A is an area of the target.

If we only take the positive area for blast impulse, the impulse can be obtained by integrating air- blast loading during duration of the positive pressure phase (i.e. from $t = t_a$ to $t = t_a + t_d$). The decay coefficient can be expressed as

$$\alpha^2 = \frac{p^o t_d \left(\alpha - 1 + e^{(-\alpha)}\right)}{I} \tag{2.13}$$

Some software, such as Blast Effect Computer Program (BEC, 2000) or ConWep (1991), can be used to predict blast loading in a different environment based on both the aforementioned equations and several experiments. These programs are usually classified to be used in military only.

Chapter III

Theoretical Background

3.1 Introduction

This chapter presents theoretical background on the relevant theories used in the formulation of the governing equations of motion of a plate subjected to blast load. The fourth-order Runge-Kutta method used in numerical integration is also shown in section 3.4 and 3.5.

3.2 Thin Plate Theory – Small Displacement

Consider a rectangular element of thin plate of dimensions dx and dy having a thickness of h subjected to a transverse distributed load of $p(x,y)$ as shown in Figure 3.1. From the classical plate theory, the moment functions M 's at the middle surface of the plate can be written in terms of transverse displacement w as

$$M_x = -D\left(\frac{\partial^2 w}{\partial x^2} + \nu\frac{\partial^2 w}{\partial y^2}\right) \tag{3.1}$$

$$M_y = -D\left(\nu\frac{\partial^2 w}{\partial x^2} + \frac{\partial^2 w}{\partial y^2}\right) \tag{3.2}$$

$$M_{xy} = M_{yx} = D(1-\nu)\frac{\partial^2 w}{\partial x \partial y} \tag{3.3}$$

where

$$D = \frac{Eh^3}{12(1-\nu^2)} \tag{3.4}$$

Here D is the bending rigidity,

ν is Poisson's ratio, and

E is the modulus of elasticity.

The out-of-plane displacement of the middle surface w is a function of coordinates x and y.

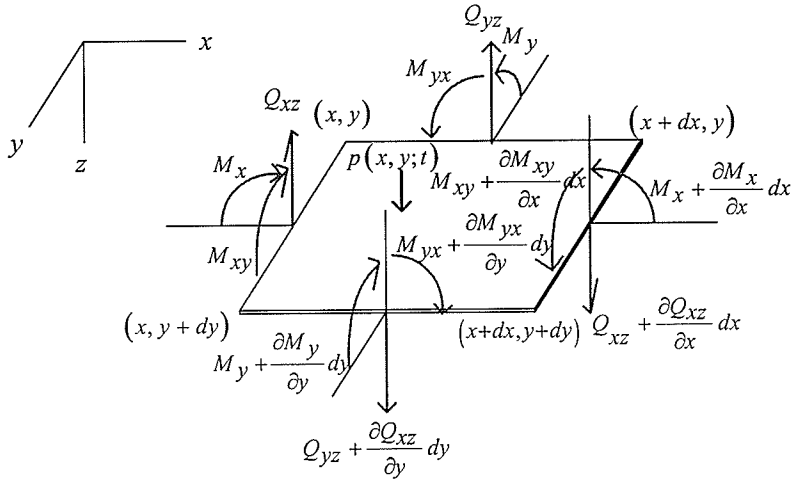

Figure 3.1 A plate element with force resultants

We can write the equilibrium of the forces in z direction, and this equation can be simplified as:

$$\frac{\partial Q_{yz}}{\partial y} + \frac{\partial Q_{xz}}{\partial x} + p(x, y, t) = 0 \tag{3.5}$$

where Q's are the transverse shear forces.

Similarly, the other two equations are

$$\frac{\partial M_y}{\partial y} - \frac{\partial M_{xy}}{\partial x} - Q_{yz} = 0 \tag{3.6}$$

$$\frac{\partial M_x}{\partial x} - \frac{\partial M_{yx}}{\partial y} - Q_{xz} = 0 \tag{3.7}$$

Substitution of Eqns. (3.1)-(3.3) into Eqns. (3.6) and (3.7) provides relations between

shear forces and the transverse displacement. The resulting relation is then substituted into Eqn. (3.5). With the application of d'Alembert principle, the equation of motion of thin plate can be written as

$$D\left(\frac{\partial^4 w}{\partial x^4}+2\frac{\partial^4 w}{\partial x^2\partial y^2}+\frac{\partial^4 w}{\partial y^4}\right)+\rho h\frac{\partial^2 w}{\partial t^2}+\mu\frac{\partial w}{\partial t}=p(x,y,t) \tag{3.8}$$

or

$$D\nabla^4 w+\rho h\frac{\partial^2 w}{\partial t^2}+\mu\frac{\partial w}{\partial t}=p(x,y,t) \tag{3.9}$$

where ρ is a mass density of the plate,

μ is a damping coefficient of the plate, and

∇^4 is a biharmonic (or bilaplacian) operator.

The aforementioned equation is a governing equation of thin plate subjected to transverse loading. The equation is valid only for small deflection.

3.3 Thin Plate Theory – Large Displacement

When the plate undergoes large deflection, in-plane normal forces have a significant effect in the analysis. Consider a small element $dx\times dy$ thin plate having thickness h in Figure 3.2. The projection of the normal forces N's and shear forces on the z axis produces a transverse load. This can be expressed as:

$$N_x\frac{\partial^2 w}{\partial x^2}+N_y\frac{\partial^2 w}{\partial y^2}+2N_{xy}\frac{\partial^2 w}{\partial x\partial y} \tag{3.10}$$

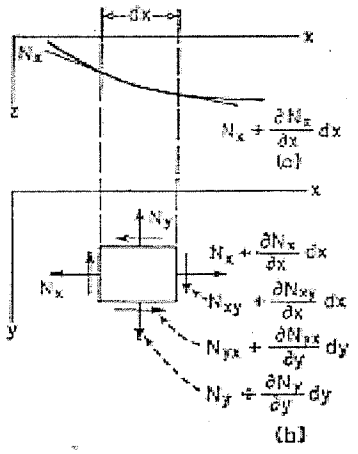

Figure 3.2 A plate element undergoes large deflection (source: Timoshenko and Woinowsky-Krieger, 1959)

The governing equation, Eqn. (3.9), now becomes

$$D\nabla^4 w+\rho h\frac{\partial^2 w}{\partial t^2}+\mu\frac{\partial w}{\partial t}=p(x,y,t)+N_x\frac{\partial^2 w}{\partial x^2}+N_y\frac{\partial^2 w}{\partial y^2}+2N_{xy}\frac{\partial^2 w}{\partial x\partial y} \tag{3.11}$$

The normal forces and in plane shear forces can be written by stress function F as

$$\begin{aligned} N_x &= h\frac{\partial^2 F}{\partial y^2} \\ N_y &= h\frac{\partial^2 F}{\partial x^2} \\ N_{xy} &= -h\frac{\partial^2 F}{\partial x\partial y} \end{aligned} \tag{3.12}$$

Upon substitution of Eqn. (3.12) into Eqn. (3.11), the von Kármán type geometric nonlinear equation (Timoshenko and Woinowsky-Krieger, 1959) for the plate is obtained as

$$D\nabla^4 w+\rho h\frac{\partial^2 w}{\partial t^2}+\mu\frac{\partial w}{\partial t}+h\left(2\frac{\partial^2 F}{\partial x\partial y}\frac{\partial^2 w}{\partial x\partial y}-\frac{\partial^2 F}{\partial y^2}\frac{\partial^2 w}{\partial x^2}-\frac{\partial^2 F}{\partial x^2}\frac{\partial^2 w}{\partial y^2}\right)=p(x,y,t) \tag{3.13}$$

Eqn. (3.13) serves as an equation of motion of thin plate undergoes large deflection.

3.4 Fourth-order Runge-Kutta Method – First-order Differential Equation

As mentioned, the Runge-Kutta method will be used in this study in the numerical integration to obtain the numerical response of the plate subjected to air-blast loading. The Runge-Kutta method is a method of numerically integrating linear and nonlinear ordinary differential equations by using a trial step at the midpoint of an interval to cancel out lower-order error terms. The fourth-order Runge-Kutta method (RK4) is the most popular method that is reasonably simple and robust and is a good general candidate for numerical solution of differential equations when combined with an intelligent adaptive step-size routine. The RK4 procedure for a first-order differentiation can be summarized as follows:

Let an example problem be specified as

$$\dot{y} = \frac{dy}{dt} = f(x, y), \quad y(t_0) = y_0 \tag{3.14}$$

Then the RK4 method for this problem is given by

$$y_{i+1} = y_i + \frac{\Delta t}{6}(k_1 + 2k_2 + 2k_3 + k_4) \tag{3.15}$$

where

$$\begin{aligned} k_1 &= f(x_i, y_i) \\ k_2 &= f\left(x_i + \frac{\Delta t}{2}, y_i + \frac{1}{2}k_1\right) \\ k_3 &= f\left(x_i + \frac{\Delta t}{2}, y_i + \frac{1}{2}k_2\right) \\ k_4 &= f(x_i + \Delta t, y_i + k_3) \end{aligned} \tag{3.16}$$

Thus, the next value y_{i+1} is determined by the present value y_i plus the product of the size of the interval Δt and an estimated slope, as in Eqn. (3.15). The estimated

slope is a weighted average of slopes: k_1 is the slope at the beginning of the interval; k_2 is the slope at the midpoint of the interval, using slope k_1 to determine the value of y at the point $t_i + \frac{\Delta t}{2}$ using Euler's method; k_3 is the slope at the midpoint, but now using the slope k_2 to determine the y-value; and k_4 is the slope at the end of the interval, with its y-value determined using k_3. In averaging the four slopes, greater weight is given to the slopes at the midpoint:

$$\text{slope} = \frac{k_1 + 2k_2 + 2k_3 + k_4}{6} \tag{3.17}$$

The RK4 method is a fourth-order method, meaning that the error per step is on the order of $(\Delta t)^5$, while the total accumulated error has order $(\Delta t)^4$.

With multi-variable, the RK4 algorithm looks similar to the aforementioned equations, except that the variables become vectors. Greenspan (2006) provided the Kutta's procedure for a second-order differential equation.

3.5 Fourth-order Runge-Kutta Method – Second-order Differential Equation

The RK4 method can also be applied to a second-order differential equation. Consider an initial value problem

$$\ddot{y} = f(x, y, \dot{y}) \tag{3.18}$$

Double-dot represents the second derivative with respect to time and over-dot is the first derivative with respect to time. The initial conditions are given as

$$y(0) = y_0,\ \dot{y}(0) = v_0 \tag{3.19}$$

Let Δt be a time interval. The problem can be converted into an equivalent system if

the following new variables are introduced

$$\begin{aligned} X_1 &= y \\ X_1' &= X_2 = \dot{y} \end{aligned} \tag{3.20}$$

Substitution of Eqn. (3.20) into Eqns. (3.18) and (3.19) yields

$$X_2' = f\left(x, y, X_2\right) \tag{3.21}$$

with initial conditions of

$$X_1(0) = y_0,\ X_2(0) = v_0 \tag{3.22}$$

The RK4's formulas are, therefore,

$$\begin{aligned} X_1(i+1) &= X_1(i) + \frac{1}{6}\left(K_1(i) + 2K_2(i) + 2K_3(i) + K_4(i)\right) \\ X_2(i+1) &= X_2(i) + \frac{1}{6}\left(M_1(i) + 2M_2(i) + 2M_3(i) + M_4(i)\right) \end{aligned} \tag{3.23}$$

where

$$\begin{aligned} K_1(i) &= (\Delta t) X_2(i) \\ K_2(i) &= (\Delta t)\left[X_2(i) + \frac{1}{2}M_1(i)\right] \\ K_3(i) &= (\Delta t)\left[X_2(i) + \frac{1}{2}M_2(i)\right] \\ K_4(i) &= (\Delta t)\left[X_2(i) + M_3(i)\right] \end{aligned} \tag{3.24}$$

and

$$\begin{aligned} M_1(i) &= (\Delta t) f\left(x(i), y(i), X_2(i)\right) \\ M_2(i) &= (\Delta t) f\left(x(i) + \frac{\Delta t}{2}, y(i) + \frac{K_1(i)}{2}, X_2(i) + \frac{1}{2}M_1(i)\right) \\ M_3(i) &= (\Delta t) f\left(x(i) + \frac{\Delta t}{2}, y(i) + \frac{K_2(i)}{2}, X_2(i) + \frac{1}{2}M_2(i)\right) \\ M_4(i) &= (\Delta t) f\left(x(i+1), y(i) + K_3(i), X_2(i) + M_3(i)\right) \end{aligned} \tag{3.25}$$

The above equations are simply two first-order differential equations, i.e. the second equation of Eqn. (3.20) and Eqn. (3.21). More simplified expressions can be obtained

by substituting Eqn. (3.24) into (3.23) and (3.25). The simplified expressions are explicitly written as

$$X_1(i+1) = X_1(i) + (\Delta t) X_2(i) + \frac{(\Delta t)}{6}\left(M_1(i) + M_2(i) + M_3(i)\right) \tag{3.26}$$

and

$$X_2(i+1) = X_2(i) + \frac{1}{6}\left(M_1(i) + 2M_2(i) + 2M_3(i) + M_4(i)\right) \tag{3.27}$$

where

$$\begin{aligned}
M_1(i) &= (\Delta t) f\left(x(i), y(i), X_2(i)\right) \\
M_2(i) &= (\Delta t) f\left(x(i) + \frac{\Delta t}{2}, y(i) + \frac{\Delta t}{2} X_2(i), X_2(i) + \frac{1}{2} M_1(i)\right) \\
M_3(i) &= (\Delta t) f\left(x(i) + \frac{\Delta t}{2}, y(i) + \frac{\Delta t}{2} X_2(i) + \frac{\Delta t}{4} M_1(i), X_2(i) + \frac{1}{2} M_2(i)\right) \\
M_4(i) &= (\Delta t) f\left(x(i+1), y(i) + \Delta t X_2(i) + \frac{\Delta t}{2} M_2(i), X_2(i) + M_3(i)\right)
\end{aligned} \tag{3.28}$$

In this study, four second-orders governing differential equations of motion were to be integrated numerically using the RK4 method. The procedure will be the same as presented in Eqns. (3.20)-(3.25).

Chapter IV

Formulation and Solutions

4.1 Statement of Problem

In this chapter, the Friedlander blast model is modified to incorporate the difference in the arrival time of the blast wave front and will first be presented. The statement of the problem will then be described. The four-mode models for both small and large displacements will be formulated.

4.2 Modified Blast Loading

In this study, we focus on the dynamic interactions between the blast wave front and the plate's surface. As mentioned in Chapter 2, if the pressure wave front arrives every point on the target almost exactly the same time, the loading on the target may be considered to distribute uniformly over the surface. However, if the arrival time for each point on this surface is different, the distribution of the loading on the target's surface at the first arrival time will be as shown in Figure 4.1. The pressure-time history of the blast loading, Eqn. (2.2), is now depending on the position on the plate and can be expressed as

$$p(x,y,t) = p^o \left[1 - \frac{t - \left(\frac{\sqrt{R^2 + x^2 + y^2}}{c_w} \right)}{t_d} \right] e^{-\alpha \frac{t - \left(\frac{\sqrt{R^2 + x^2 + y^2}}{c_w} \right)}{t_d}} \qquad (4.1)$$

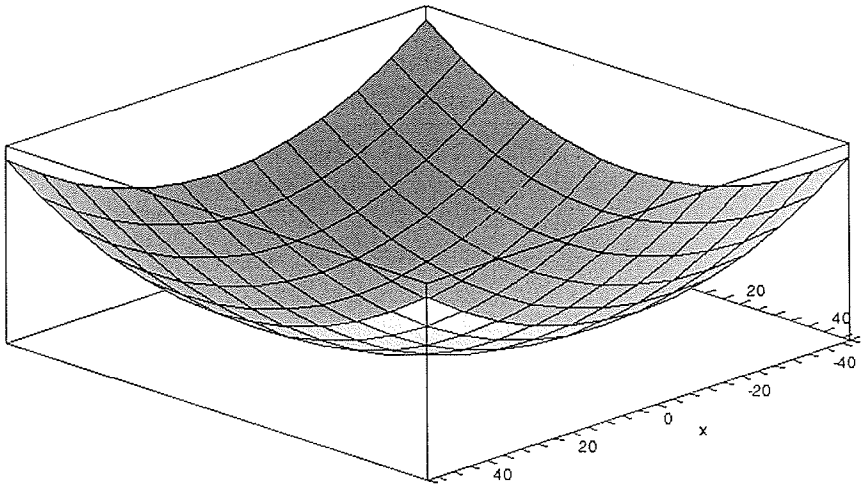

Figure 4.1 A shock wave front on a target's surface at the first arrival time

Figures 4.2 illustrates the integration of the pressure-time histories of the same blast loading on a plate's surface having different radial distance-to-plate's dimension ratio ($R/(a/2)$: where a is the largest plate dimension) evaluated using Eqns. (2.2) and (4.1)).

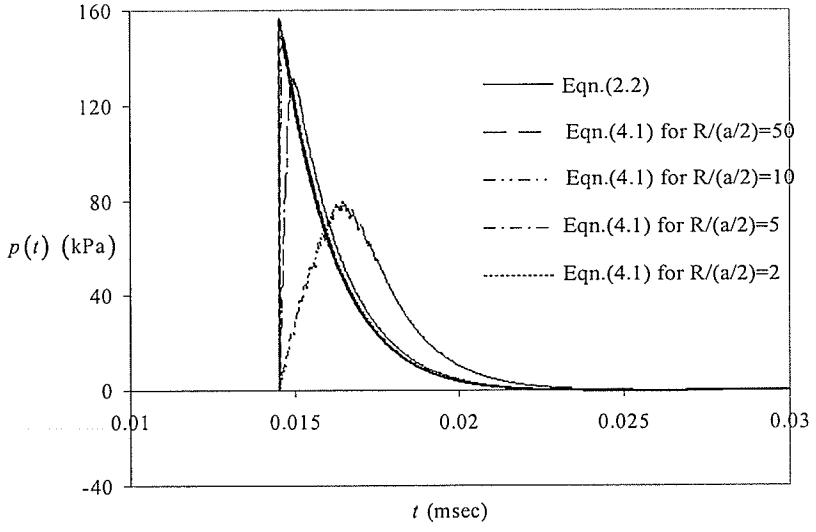

Figure 4.2 Comparison of the pressure-time histories on a plate's surface with different radial distance-to-plate's dimension $R/(a/2)$ ratio

4.3 Statement of Problem

Figure 4.3 shows a rectangular plate having a length of a, width of b, and a thickness of h. The plate is fully clamped on all edges. This plate is subjected to air-blast loading in the out-of-plane direction.

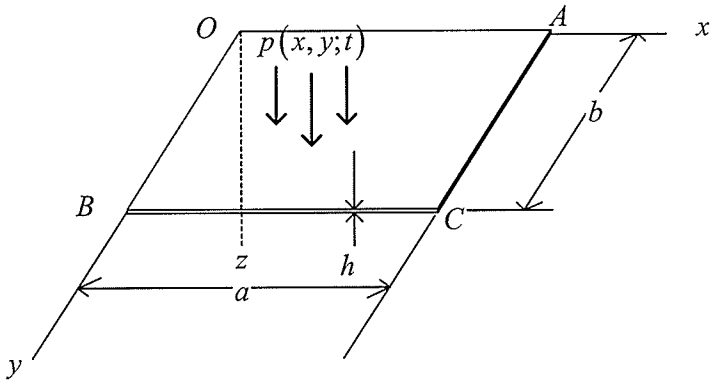

Figure 4.3 A thin plate subjecting to air-blast loading

Let u, v, and w be the displacements of a point at the middle surface in the x, y, and z directions, respectively. The clamped boundary conditions are given by

$$\begin{aligned} w = \frac{\partial w}{\partial x} = 0 \quad & \text{at } x = 0 \text{ and } x = a \\ w = \frac{\partial w}{\partial y} = 0 \quad & \text{at y} = 0 \text{ and } y = b \end{aligned} \tag{4.2}$$

The stress boundary conditions require that the stress function F satisfies the following conditions:

$$\begin{aligned} \frac{\partial F}{\partial x} = 0 \quad & \text{at } x = 0 \text{ and } x = a \\ \frac{\partial F}{\partial y} = 0 \quad & \text{at y} = 0 \text{ and } y = b \end{aligned} \tag{4.3}$$

The compatibility condition is

$$\nabla^4 F = E\left[\left(\frac{\partial^2 w}{\partial x \partial y}\right)^2 - \frac{\partial^2 w}{\partial x^2}\frac{\partial^2 w}{\partial y^2}\right] \tag{4.4}$$

4.4 Four-mode Model Displacement Function – Equations of Motion

Since the boundaries are secured, neither translation nor pivoting is allowed. The displacement function can be chosen from the shape function that satisfies the clamped boundary conditions. With this, the displacement function for clamped plate can be expressed as:

$$w(x,y,t)=\sum_{m=1}^{\infty}\sum_{n=1}^{\infty}w_{mn}(t)\left(1-\cos\frac{m\pi x}{a}\right)\left(1-\cos\frac{n\pi y}{b}\right) \tag{4.5}$$

Here $w_{mn}(t)$ will be time-dependent amplitude. Although the solution contains a infinite number of terms or modes, only those first few modes are dominating modes. In this study, four modes are chosen because the problem is symmetric with respect to the centre of the plate. The solution, Eqn. (4.5), can be explicitly written as

$$\begin{aligned} w(x,y,t)=w_{22}(t)\left(1-\cos\frac{2\pi x}{a}\right)\left(1-\cos\frac{2\pi y}{b}\right)+w_{26}(t)\left(1-\cos\frac{2\pi x}{a}\right)\left(1-\cos\frac{6\pi y}{b}\right) \\ +w_{62}(t)\left(1-\cos\frac{6\pi x}{a}\right)\left(1-\cos\frac{2\pi y}{b}\right)+w_{66}(t)\left(1-\cos\frac{6\pi x}{a}\right)\left(1-\cos\frac{6\pi y}{b}\right) \end{aligned} \tag{4.6}$$

Substituting the above displacement function into the compatibility condition, Eqn. (4.4), the explicit stress function for large displacement problem satisfying all edge clamped boundary conditions is

$$
\begin{aligned}
F = {} & F_1 \cos(\frac{12\pi x}{a}) \cos(\frac{2\pi y}{b}) + F_2 \cos(\frac{2\pi y}{b}) + F_3 \cos(\frac{4\pi x}{a}) \cos(\frac{8\pi y}{b}) + \\
& F_4 \cos(\frac{4\pi x}{a}) \cos(\frac{4\pi y}{b}) + F_5 \cos(\frac{8\pi x}{a}) \cos(\frac{6\pi y}{b}) + F_6 \cos(\frac{8\pi x}{a}) + \\
& F_7 \cos(\frac{6\pi x}{a}) \cos(\frac{8\pi y}{b}) + F_8 \cos(\frac{6\pi y}{b}) \cos(\frac{4\pi y}{b}) + F_9 \cos(\frac{6\pi x}{a}) \cos(\frac{12\pi y}{b}) + \\
& F_{10} \cos(\frac{8\pi x}{a}) \cos(\frac{4\pi y}{b}) + F_{11} \cos(\frac{8\pi x}{a}) \cos(\frac{8\pi y}{b}) + F_{12} \cos(\frac{2\pi x}{a}) + \\
& F_{13} \cos(\frac{6\pi x}{a}) \cos(\frac{2\pi y}{b}) + F_{14} \cos(\frac{8\pi x}{a}) \cos(\frac{2\pi y}{b}) + F_{15} \cos(\frac{2\pi x}{a}) \cos(\frac{6\pi y}{b}) + \\
& F_{16} \cos(\frac{2\pi x}{a}) \cos(\frac{8\pi y}{b}) + F_{17} \cos(\frac{2\pi x}{a}) \cos(\frac{4\pi y}{b}) + F_{18} \cos(\frac{2\pi x}{a}) \cos(\frac{12\pi y}{b}) + \\
& F_{19} \cos(\frac{2\pi x}{a}) \cos(\frac{2\pi y}{b}) + F_{20} \cos(\frac{4\pi x}{a}) \cos(\frac{2\pi y}{b}) + F_{21} \cos(\frac{6\pi x}{a}) \cos(\frac{6\pi y}{b}) + \\
& F_{22} \cos(\frac{12\pi y}{b}) + F_{23} \cos(\frac{12\pi x}{a}) + F_{24} \cos(\frac{12\pi x}{a}) \cos(\frac{4\pi y}{b}) + \\
& F_{25} \cos(\frac{12\pi x}{a}) \cos(\frac{6\pi y}{b}) + F_{26} \cos(\frac{8\pi y}{b}) + F_{27} \cos(\frac{4\pi x}{a}) \cos(\frac{6\pi y}{b}) + \\
& F_{28} \cos(\frac{4\pi x}{a}) \cos(\frac{12\pi y}{b}) + F_{29} \cos(\frac{4\pi y}{b}) + F_{30} \cos(\frac{12\pi x}{a}) \cos(\frac{8\pi y}{b}) + \\
& F_{31} \cos(\frac{4\pi x}{a}) + F_{32} \cos(\frac{6\pi x}{a}) + F_{33} \cos(\frac{6\pi y}{b}) + F_{34} \cos(\frac{8\pi x}{a}) \cos(\frac{12\pi y}{b})
\end{aligned}
\tag{4.7}
$$

where explicit F_m are given in Appendix A.

Substituting the stress function, Eqn. (4.7), and the displacement function, Eqn. (4.6), into the equation of motion for a large displacement, Eqn. (3.13), and minimizing error function using the Galerkin method, the following system of differential equations of motion are obtained.

$$
\begin{aligned}
&\ddot{w}_{22} - V_1 w_{22}^{\ 3} - V_2 w_{22}^{\ 2} w_{26} - V_3 w_{22}^{\ 2} w_{62} - V_4 w_{66} w_{22}^{\ 2} - V_5 w_{22} w_{26}^{\ 2} - V_6 w_{22} w_{62}^{\ 2} - \\
&V_7 w_{22} w_{66}^{\ 2} - V_8 w_{22} w_{26} w_{62} - V_9 w_{66} w_{22} w_{26} - V_{10} w_{66} w_{22} w_{62} - V_{11} w_{22} - V_{12} w_{26}^{\ 3} - \\
&V_{13} w_{26}^{\ 2} w_{62} - V_{14} w_{66} w_{26}^{\ 2} - V_{15} w_{26} w_{62}^{\ 2} - V_{16} w_{26} w_{66}^{\ 2} - V_{17} w_{66} w_{62} w_{26} - V_{18} w_{26} - \\
&V_{19} w_{62}^{\ 3} - V_{20} w_{66} w_{62}^{\ 2} - V_{21} w_{62} w_{66}^{\ 2} - V_{22} w_{62} - V_{23} w_{66}^{\ 3} - V_{24} w_{66} - V_{25} \dot{w}_{22} - V_{26} P_1 = 0 \\
&\ddot{w}_{26} - V_{27} w_{22}^{\ 3} - V_{28} w_{22}^{\ 2} w_{26} - V_{29} w_{22}^{\ 2} w_{62} - V_{30} w_{66} w_{22}^{\ 2} - V_{31} w_{22} w_{26}^{\ 2} - V_{32} w_{22} w_{62}^{\ 2} - \\
&V_{33} w_{22} w_{66}^{\ 2} - V_{34} w_{22} w_{26} w_{62} - V_{35} w_{66} w_{22} w_{26} - V_{36} w_{66} w_{22} w_{62} - V_{37} w_{22} - V_{38} w_{26}^{\ 3} - \\
&V_{39} w_{26}^{\ 2} w_{62} - V_{40} w_{66} w_{26}^{\ 2} - V_{41} w_{26} w_{62}^{\ 2} - V_{42} w_{26} w_{66}^{\ 2} - V_{43} w_{66} w_{62} w_{26} - V_{44} w_{26} - \\
&V_{45} w_{62}^{\ 3} - V_{46} w_{66} w_{62}^{\ 2} - V_{47} w_{62} w_{66}^{\ 2} - V_{48} w_{62} - V_{49} w_{66}^{\ 3} - V_{50} w_{66} - V_{51} \dot{w}_{26} - V_{52} P_2 = 0 \\
&\ddot{w}_{62} - V_{53} w_{22}^{\ 3} - V_{54} w_{22}^{\ 2} w_{26} - V_{55} w_{22}^{\ 2} w_{62} - V_{56} w_{66} w_{22}^{\ 2} - V_{57} w_{22} w_{26}^{\ 2} - V_{58} w_{22} w_{62}^{\ 2} - \\
&V_{59} w_{22} w_{66}^{\ 2} - V_{60} w_{22} w_{26} w_{62} - V_{61} w_{66} w_{22} w_{26} - V_{62} w_{66} w_{22} w_{62} - V_{63} w_{22} - V_{64} w_{26}^{\ 3} - \\
&V_{65} w_{26}^{\ 2} w_{62} - V_{66} w_{66} w_{26}^{\ 2} - V_{67} w_{26} w_{62}^{\ 2} - V_{68} w_{26} w_{66}^{\ 2} - V_{69} w_{66} w_{62} w_{26} - V_{70} w_{26} - \\
&V_{71} w_{62}^{\ 3} - V_{72} w_{66} w_{62}^{\ 2} - V_{73} w_{62} w_{66}^{\ 2} - V_{74} w_{62} - V_{75} w_{66}^{\ 3} - V_{76} w_{66} - V_{77} \dot{w}_{62} - V_{78} P_3 = 0 \\
&\ddot{w}_{66} - V_{79} w_{22}^{\ 3} - V_{80} w_{22}^{\ 2} w_{26} - V_{81} w_{22}^{\ 2} w_{62} - V_{82} w_{66} w_{22}^{\ 2} - V_{83} w_{22} w_{26}^{\ 2} - V_{84} w_{22} w_{62}^{\ 2} - \\
&V_{85} w_{22} w_{66}^{\ 2} - V_{86} w_{22} w_{26} w_{62} - V_{87} w_{66} w_{22} w_{26} - V_{88} w_{66} w_{22} w_{62} - V_{89} w_{22} - V_{90} w_{26}^{\ 3} - \\
&V_{91} w_{26}^{\ 2} w_{62} - V_{92} w_{66} w_{26}^{\ 2} - V_{93} w_{26} w_{62}^{\ 2} - V_{94} w_{26} w_{66}^{\ 2} - V_{95} w_{66} w_{62} w_{26} - V_{96} w_{26} - \\
&V_{97} w_{62}^{\ 3} - V_{98} w_{66} w_{62}^{\ 2} - V_{99} w_{62} w_{66}^{\ 2} - V_{100} w_{62} - V_{101} w_{66}^{\ 3} - V_{102} w_{66} - V_{103} \dot{w}_{66} - V_{104} P_4 = 0
\end{aligned}
\tag{4.8}
$$

where explicit V_m and P_m are given in Appendices B and C, respectively.

Similarly for the small displacement problem, the set of equations of motion can be obtained by substituting the displacement function, Eqn. (4.6), into the equation of motion, Eqn. (3.9), and applying the Galerkin method into the resulting equations. The process yields the following equations of motion for thin plate with small displacement:

$$
\begin{aligned}
&\ddot{w}_{22} - J_1 w_{22} - J_2 w_{26} - J_3 w_{62} - J_4 w_{66} + J_5 \dot{w}_{22} - J_6 P_1 = 0 \\
&\ddot{w}_{26} - J_7 w_{22} - J_8 w_{26} - J_9 w_{62} - J_{10} w_{66} + J_{11} \dot{w}_{26} - J_{12} P_2 = 0 \\
&\ddot{w}_{62} - J_{13} w_{22} - J_{14} w_{26} - J_{15} w_{62} - J_{16} w_{66} + J_{17} \dot{w}_{62} - J_{18} P_3 = 0 \\
&\ddot{w}_{66} - J_{19} w_{22} - J_{20} w_{26} - J_{21} w_{62} - J_{22} w_{66} + J_{23} \dot{w}_{66} - J_{24} P_4 = 0
\end{aligned}
\tag{4.9}
$$

where explicit J_m are given in Appendix D.

Eqns. (4.8) and (4.9), after integrating over the plate surface area, are the set of ordinary differential equations which can be used to solve the thin plate subjected to

air-blast loading. Note that, for large displacement, the differential equations are nonlinear while, the differential equations are linear for small displacement. The RK4 method is used to solve the governing equations in this study. The approximation integration of an air-blast loading is obtained by using the Gaussian quadrature. This is done by dividing the plate into numbers of grid element. Five gauss point double integration is used. The resulting load is then averaged over the plate's area for each time step of integration in the RK4.

Chapter V

Numerical Results and Discussion

5.1 Introduction

As mentioned in Chapter 4, the equations of motion were solved numerically using RK4. The time step of integration Δt was chosen to be 0.01 m-sec unless otherwise stated. Computer programs were written in FORTRAN language to perform the analyses of the four-mode model presented in the previous chapter. The program code is listed in Appendix E. This chapter presents the numerical results of the analyses. The results were first compared with the existing experimental and finite element results to validate the proposed solutions. The effects that the plate aspect ratio, the plate size, and the charge location had on the response of the plate were investigated.

5.2 The Modified Friedlander Model

As mentioned in Section 4.2, the dynamic interactions of the blast wave front with the plate's surface are described by the difference in the arrival time of the wave front at the plate's surface. This modified Friedlander model is expressed as in Eqn. (4.1) and is depicted in Figure 4.3.

Figures 5.1 and 5.2 show the variation of the percentage difference of the peak pressure averaged over the plate's surface area and the variation of the percentage difference of the maximum impulse with the Friedlander model when the $R/(a/2)$

changes. It can be seen that for a small values of $R/(a/2)$, an increase in the $R/(a/2)$ decreases the average peak pressure while for a large value of $R/(a/2)$, an increase value of $R/(a/2)$ does not significantly decrease the average peak pressure. The peak pressure is approximating constant when $R/(a/2)$ is lager than 20. The percentage difference of the maximum impulse varies within only 2% when the $R/(a/2)$ changes. Therefore, the change in the $R/(a/2)$ does not have much effect on the maximum impulse.

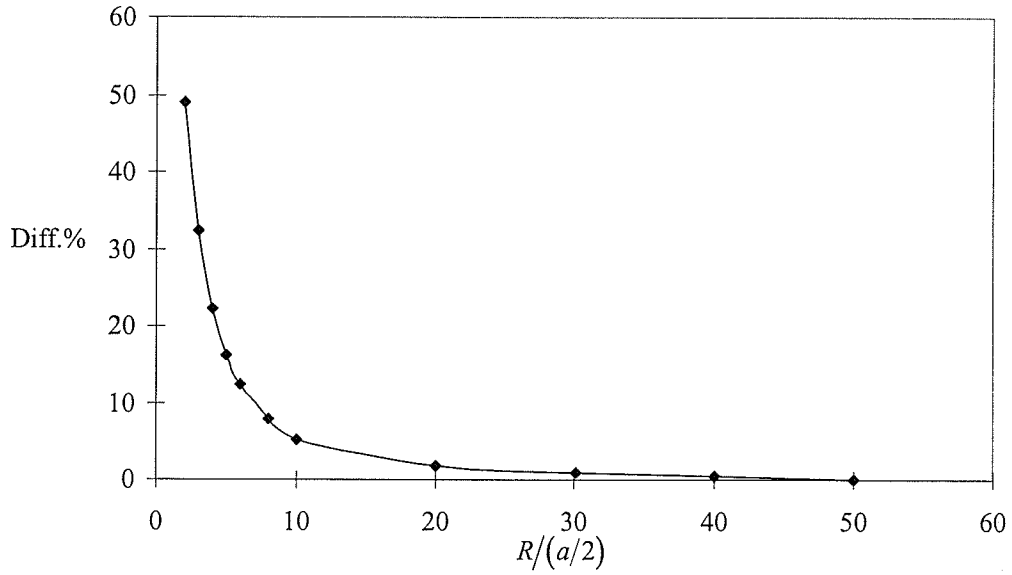

Figure 5.1 The variation of the percentage difference of the peak pressure averaged over the plate's surface area when the $R/(a/2)$ changes

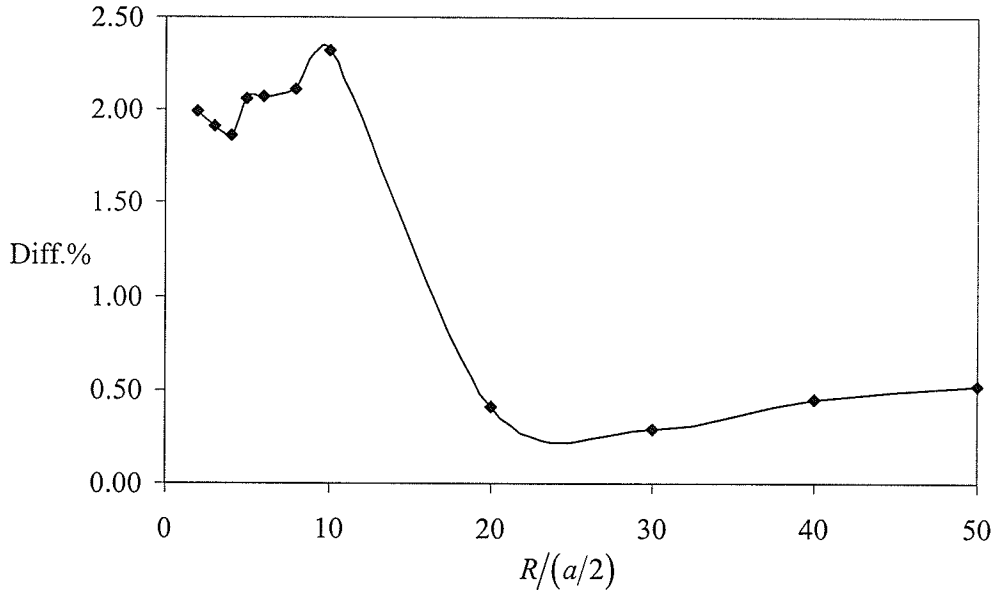

Figure 5.2 The variation of the percentage difference of the impulse when the $R/(a/2)$ changes

5.3 Validation

Several experimental tests on clamped square thin steel plates subjected to air-blast loading were conducted by Houlston and slater (1987). Only two test results, namely test 1 and test 2, were chosen for a comparison purpose here. This is due to the fact that either there were no pressure-time histories given in other tests or the response of the experiments showed plastic deformation which is not in the scope of this thesis. The geometric and material properties of the square plate are given as (Houlston and Slater, 1987):

Plate width and length: a = 508 mm;

Plate thickness: h = 3.4 mm;

Poisson ratio: ν = 0.3;

Young's modulus: E = 207 GPa;

Mass density: ρ = 7770 kg/m^3.

The damping ratio and natural frequencies were not given in their paper. In this study, it was assumed that:

Damping ratio: ξ = 2.2%;

Natural frequency: ω = 35.99 rad /s.

As mentioned in the scope, the temperature effects were ignored in this study. As a consequence, all material properties of the steel plate were assumed to remain constant in the analyses.

The experimental results of test 1 and test 2 from Houlston et al. (1985) and Houlston and Desrochers (1987) are summarized in Table 5.1. The pressure-time histories of test 1 and test 2 are shown in Figures 5.3 and 5.4, respectively. The Friedlander model was used to simulate the pressure-time histories in the four-mode model. Since the maximum displacement in test 1 was only 1% of the plate width, small displacement analysis, Eqn. (4.9), was used for test 1. The maximum displacement in test 2 was 2% of the plate width and the peak overpressure was three times the peak overpressure recorded in test 1, large displacement analysis, Eqn. (4.8), was used for test 2. At-rest initial conditions (i.e. zero displacement and velocity at the arrival time of the blast wave) were used in the analyses of both cases.

Table 5.1 Summary of experimental results from Houlston et al. (1985) and Houlston and Desrochers (1987)

Test	Overpressure (kPa)	Pulse duration (ms)	Maximal displacement (mm)
1	55	2.0	5.42
2	172	2.0	11.47

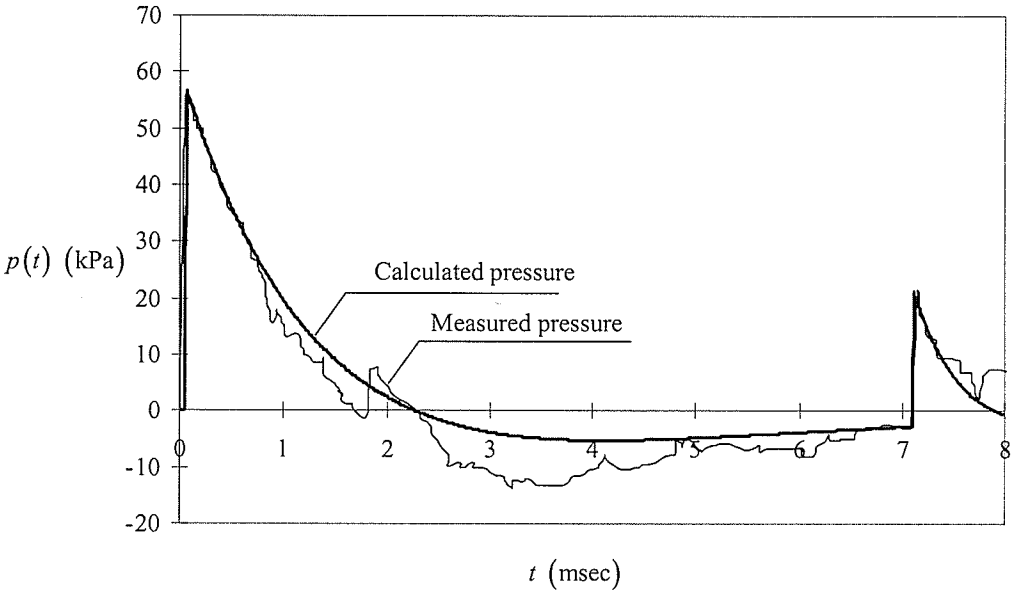

Figure 5.3 The pressure-time history for test 1 (Houlston et al., 1985)

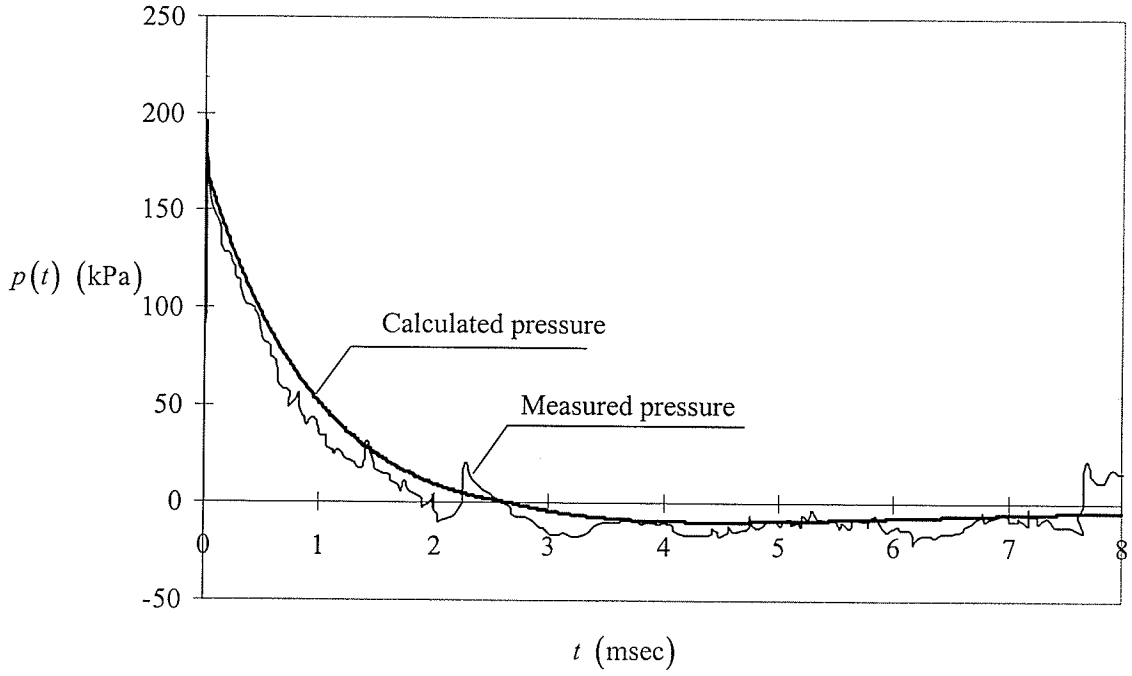

Figure 5.4 The pressure-time history for test 2 (Houlston and Desrochers, 1987)

Figure 5.5 illustrates a comparison of a displacement time-history of the point at the centre of the plate for test 1. ADINA results were taken from Houlston et al.'s paper. In Houlston et al.'s, Newmark's time integration method and linear elastic analysis were employed. As seen in the figure, the present model provided an extremely accurate prediction of the plate's response especially in the forced vibration zone, compared to the experimental results. There are, however, some discrepancies in the maximum responses in the free-vibration zone between those obtained from the present model and the experimental results, such as at approximately 8 msec. The predicted values from the present model and from ADINA are similar in the free-vibration zone.

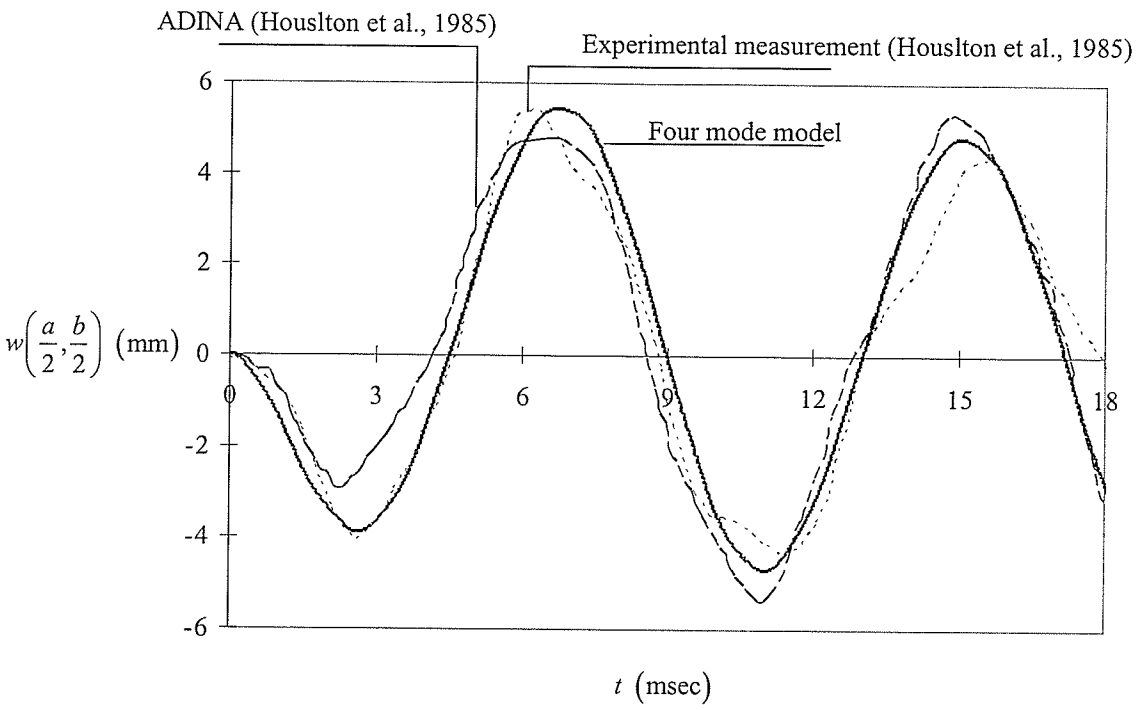

Figure 5.5 A displacement time-history of a centre point of the plate for test 1

Figure 5.6 shows a displacement time-history at the centre point for test 2. Houlston and Desrochers (1987) employed nonlinear finite-element analysis in ADINA together with Newmark's method in their numerical analysis. The present model's prediction of the displacement time-history agrees very well with the results obtained experimentally, and with the prediction provided by ADINA. In fact, the four-mode model predicted the maximum displacements to be closer to the experimental values than ADINA. Also notable in Figure 5.3 is that both ADINA and the four-mode model provide a trend of over-prediction of the displacement in the free-vibration zone. This may be due to the fact that both analyses did not consider the temperature effects. As mentioned in Section 1.2, temperature rise from blast affects the response of metal structures since the temperature rise alters material properties.

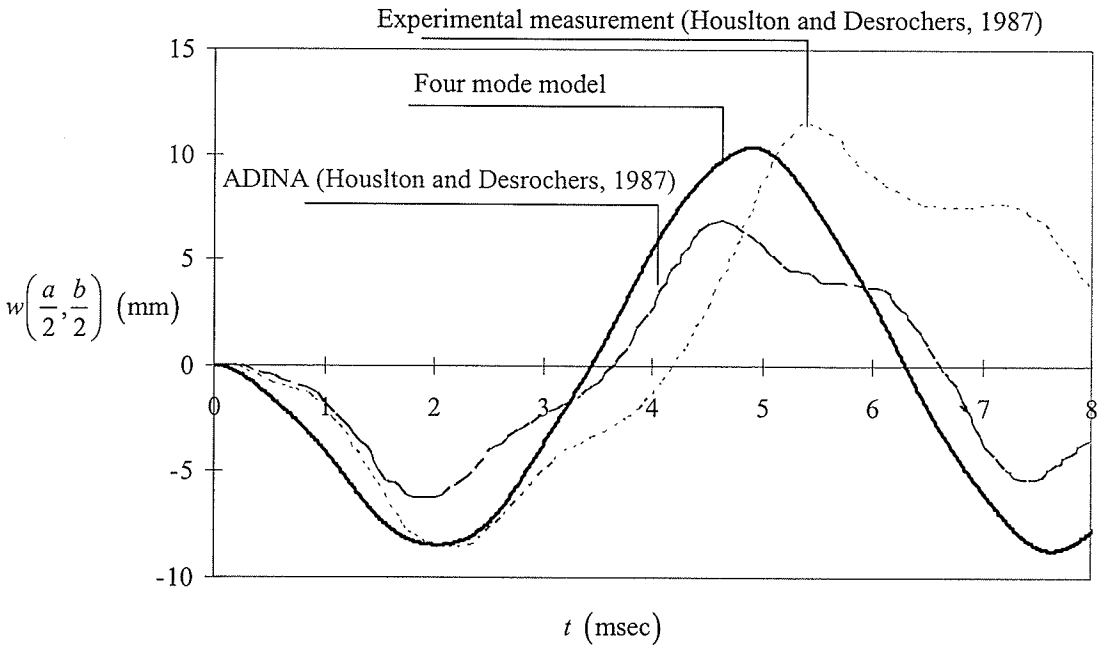

Figure 5.6 A displacement time-history at centre for test 2

So far, the loading considered was assumed to be uniformly distributed over the plate's surface. Figures 5.7 and 5.8 present comparisons of the responses for test 1 and test 2 obtained using a uniformly distributed pressure Friedlander distribution, defined by Eqn. (2.2), and the modified Friedlander distribution, defined by Eqn. (4.1), respectively. The radial distance-to-plate's dimension ratios for the problems are 12.0 and 9.6, and the scaled distances Z are 6.31 and 3.32 for test 1 and test 2, respectively. At first glance, the responses from both models were almost identical. Nonetheless, detailed investigation (see Table 5.2) indicates that the use of the modified Friedlander model in pressure distribution provided a little better prediction of the plate's response than the Friedlander model for both tests.

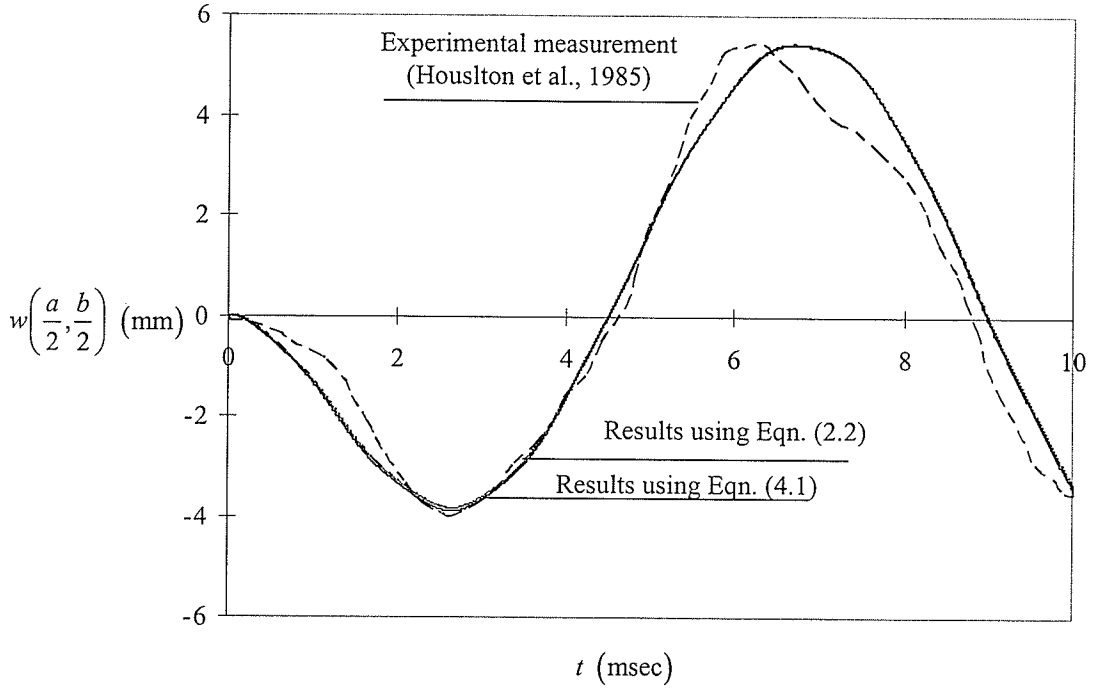

Figure 5.7 A comparison of the displacement time-histories obtained from the Friedlander model and the modified Friedlander model for test 1

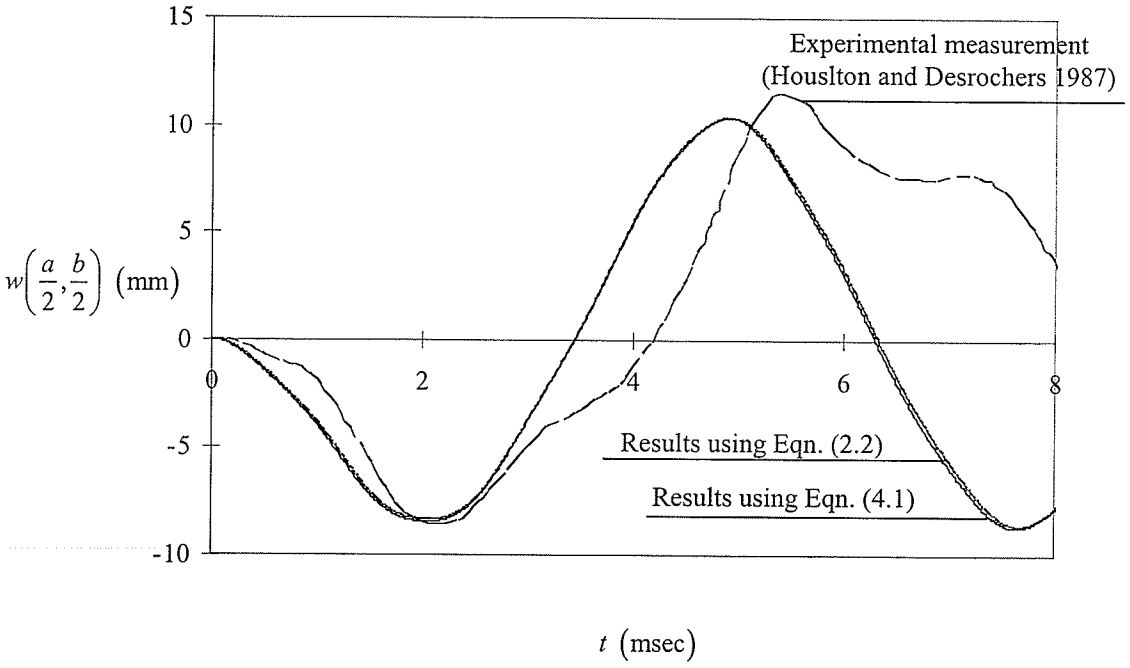

Figure 5.8 A comparison of the displacement time-histories obtained from the Friedlander model and the modified Friedlander model for test 2

Table 5.2 A comparison of peak displacements using the Friedlander and the modified Friedlander models

		Results from the Friedlander Model		Results from the modified Friedlander Model	
		Negative peak	Positive peak	Negative peak	Positive peak
Test 1	Present Model	-3.85	5.40	-3.89	5.45
	Experimental Measurement	-4.0	5.42	-4.00	5.42
	Diff. (%)	3.83	0.37	2.69	0.47
Test 2	Present Model	-8.39	10.32	-8.45	10.36
	Experimental Measurement	-8.59	11.47	-8.59	11.47
	Diff. (%)	2.43	10.67	1.64	9.71

5.3 Numerical Examples

To demonstrate the applicability of the model and to further investigate the effects of some parameters on the response of plates subjected to blast load, numerical examples are presented in this section. The first example investigates the effects of a plate's aspect ratio on the response of the plate to a blast load. The second example is to investigate what effect of the plate's area has on the response of the plate to a blast

loading. The third example considers the effect that the charge location has on the response of the plate to a blast load. The last example considers the effect that the radial distance-to-plate's dimension has on the response of the plate for peak displacement and acceleration. In all examples, the thickness of the plate was assumed to be 3.4 mm and the material properties are the same as those in the previous section.

5.3.1 Plate's Aspect Ratio

In this example, a thin plate of varying aspect ratio $\lambda = a/b$, where a is the length and b is the width, was considered. The plate has a surface area of 258064 mm^2. Both linear and nonlinear analysis was conducted. For linear analysis, an air-blast having the same peak overpressure as test 1 in the previous section was used in the modified Friedlander distribution. For nonlinear analysis, the air-blast was assumed to have the same peak overpressure as test 2 in the previous section. Figure 5.9 illustrate the effect that the plate's aspect ratio, varying from 0.1 to 1.0 with an increment of 0.1, has on the maximum displacement of the plate for both linear and nonlinear analyses. It can be seen that an increase in the plate's aspect ratio increases the maximum displacement of the plate. The increase in the maximum displacement decreases when the plate's aspect ratio is close to unity. This relationship implies that a square plate is the weakest configuration in sustaining the air-blast loading.

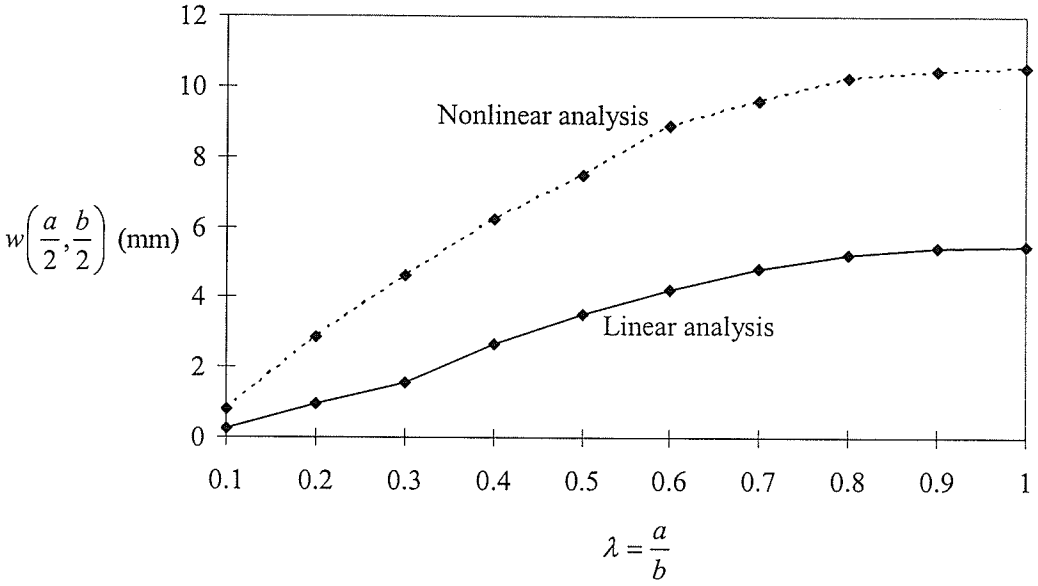

Figure 5.9 The effect of the plate's aspect ratio on the maximum deflection of the plate

5.3.2 Plate's Area

The effects of the plate area on the maximum displacement of the plate subjected to air-blast loading were examined. The plate thickness and material properties were chosen to be the same as those used in Section 5.2. The plate's aspect ratio was selected to be unity from the results of the previous example. The peak overpressure in the linear analysis was the same as that in the previous example. For nonlinear analysis, however, the peak overpressure was chosen to be less than that used in the previous example. This was to avoid plastic deformation that might occur in the plate, in order to remain within the scope of the present study. The new loading parameters were introduced as follows:

Mach number: M = 1.279;

Local speed of sound: c_s = 340.29 m/sec;

The peak reflected overpressure, p^o = 150 kPa;

Positive phase duration: t_d = 2 ms;

Decay coefficient: α = 1.0;

Stand-off or radial distance: R = 1 m.

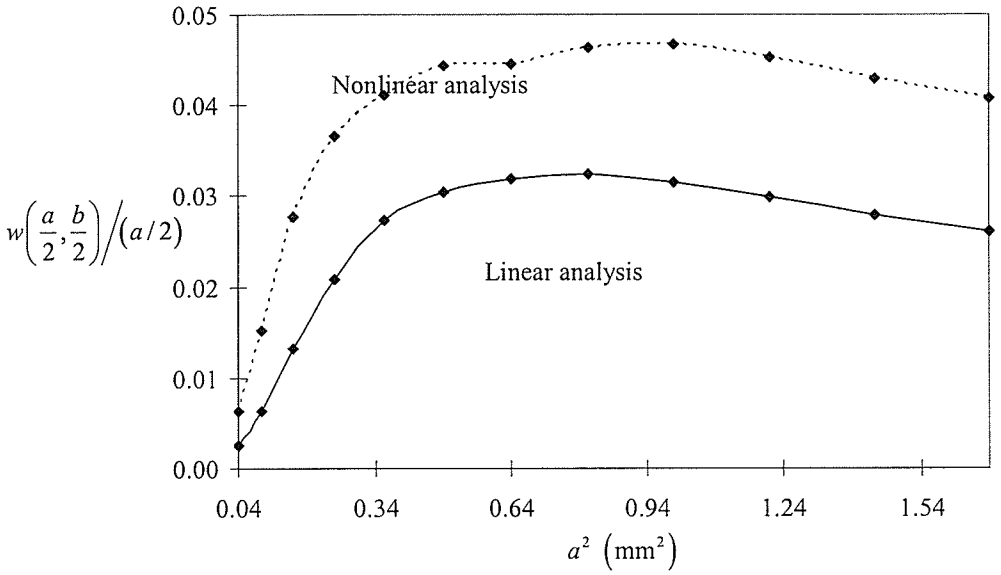

Figure 5.10 The effects of plate area on the flexibility of the plate

Figure 5.10 illustrates the effects of the plate area on the flexibility of the plate (demonstrated by the slope of the chord connecting the edge of the plate and the point at the centre of the plate) in both the linear and nonlinear analysis. First, an increase in the plate area increases the flexibility of the plate. When the dimension of the plate is approximately 900 × 900 mm^2, the plate's flexibility starts to drop. Further increases in the plate area proved to decrease the flexibility of the plate. Similar to the case of linear analysis, an increase in the plate area increases the flexibility of the plate until the plate dimension reaches 1000 × 1000 mm^2. Further increase in the area decreases the flexibility of the plate.

5.3.3 *Location of the Charge*

The effect the charge location has on the maximum displacement of the plate subjected to air-blast loading was investigated. The plate was assumed to be square with an effective dimension of 1000 mm × 1000 mm. The choice was made from previous two examples, seeing that the plate was found to produce the largest maximum displacement when the aspect ratio of the plate was unity and the dimensions were 1000 mm × 1000 mm. Only nonlinear analysis was considered in this example. The projections of the charge locations on the plate were chosen to be on the edge *OA* and on the diagonal line *OC* as shown in Figure 5.11. Figure 5.12 shows displacement profile of the plate at time $t = 9.62$ msec when the projection of the charge location is at point 5 on the *OA* line. Figure 5.13 shows the plots of the displacement at the plate centre and the projections of the charge locations on the plate. When the charge is above the mid-length of the edge or the mid-length of the diagonal line, the displacement at the centre of the plate is the largest. The displacement at the centre is the largest when the charge is directly above the centre of the plate. The difference in the values of the displacement at the centre of the plate for the different locations of the charge is very small, only 0.04%. Since the effects of the location of the charge are very small, linear analysis was not included here.

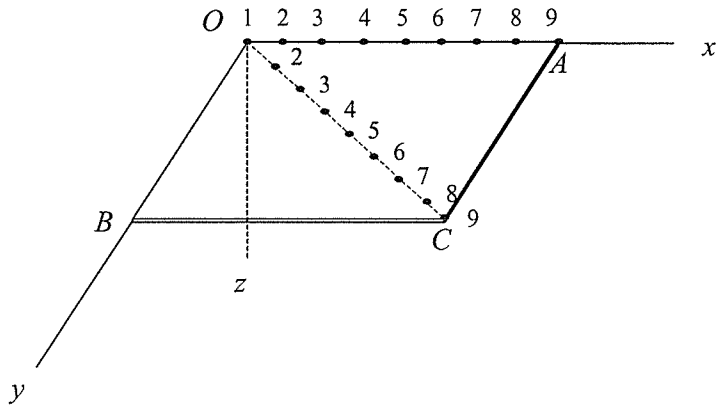

Figure 5.11 Projections of charge location on the plate

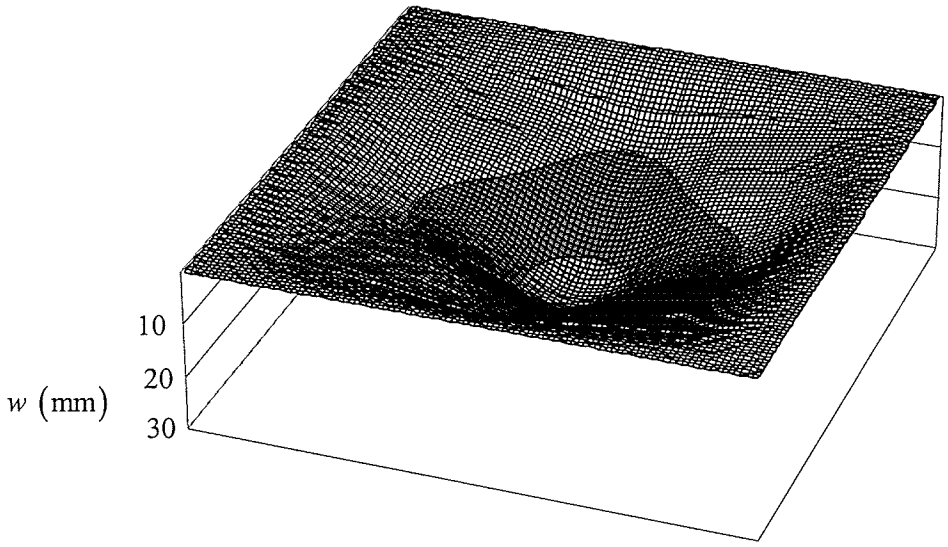

Figure 5.12 Displacement profile of the plate at time $t = 9.62$ msec when the charge is at point 5 on the OA line

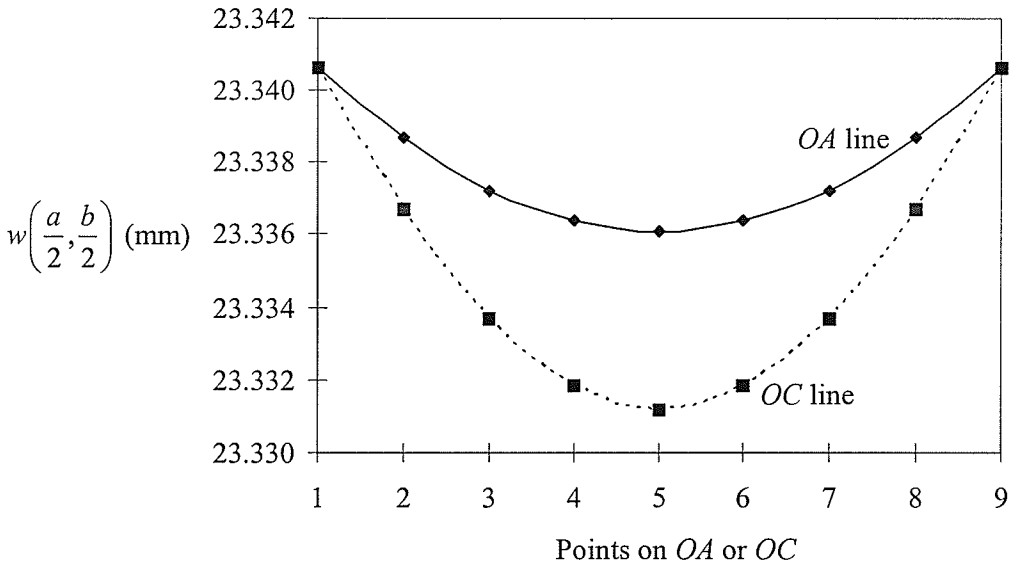

Figure 5.13 Displacement at the plate centre and the charge projections on the plate

5.3.4 Radial Distance-to-Plate's Dimension

In this example, we compare results obtained using the modified Friedlander model, Eqn. (4.1), with results obtained using the Friedlander model, Eqn. (2.2), to investigate the effect of radial distance-to-plate's dimension on the peak displacement and acceleration. The blast loading used here is the same as mentioned before in section 4.2. Only nonlinear analysis was considered in this example. Figure 5.14 shows the variation of the percentage difference of the peak displacement when the $R/(a/2)$ changes. An increase in the value of $R/(a/2)$ reduces the percentage difference. However, most of values are smaller than 3%. Therefore, we do not have to consider the effect the dynamic interactions of the blast wave front with the plate surface expect when $R/(a/2)$ is smaller than 3.

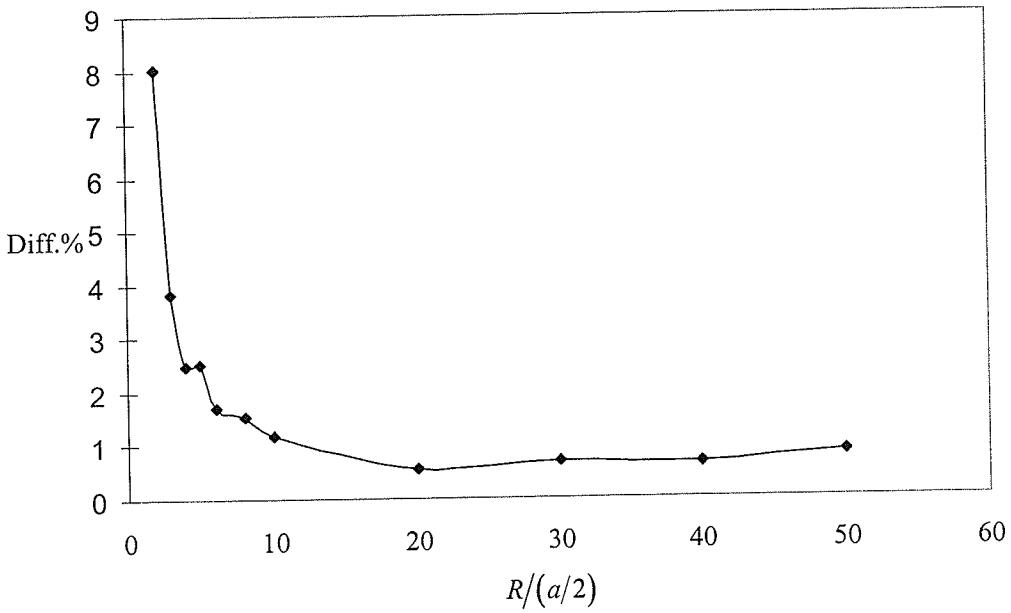

Figure 5.14 The effect of radial distance-to-plate's dimension on the peak displacement

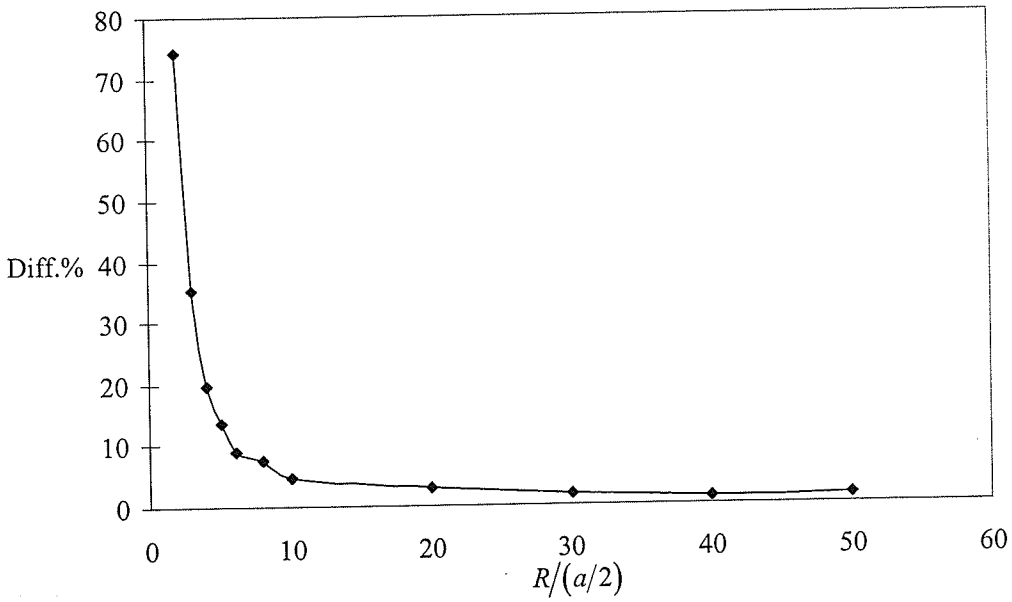

Figure 5.15 The effect of radial distance-to-plate's dimension on the peak acceleration

Figure 5.15 shows the variation of the percentage difference of the peak acceleration when the $R/(a/2)$ changes. An increases in the value of $R/(a/2)$ reduces the percentage difference and the percentage difference is 4.53% when $R/(a/2)$ equal 10. Thus we have to use the modified Friedlander model to calculate the acceleration when the $R/(a/2)$ ratio is smaller or equal to 10.

From the Figure 5.1, 5.2, 5.13, and 5.14, it can be seen that the maximum displacement depends on the maximum impulse and the maximum acceleration depends on the peak pressure.

Chapter VI

Conclusion and Recommendation

6.1 Conclusion

The linear and nonlinear analysis of a fully clamped large thin plate subjected to air-blast loading was presented. The blast load was assumed to be distributed over the surface area of the plate. The linear equation of motion was based on the classical thin plate theory and the nonlinear equations of motion were based on the von Kármán geometric nonlinear theory. The four-mode solution was assumed. The governing equations of motion were formulated using the Galerkin technique and solved numerically by the fourth-order Runge-Kutta method. In the modeling of an air-blast overpressure on a plate surface, the Friedlander distribution was used. The Friedlander model was also modified to incorporate the dynamic interactions between the blast wave front and the plate's surface. The integration of the loading from the modified Friedlander model over the area was carried out using the Gaussian quadrature. The numerical results from the use of the present four-mode model, together with the modified Friedlander and the Friedlander models were validated with the existing experimental results.

From the study, the following conclusion can be made:

- The modified Friedlander can be used to provide a good approximation of the air-blast distribution on the plate.

- The peak pressure calculated from the modified Friedlander model depends on the $R/(a/2)$.

- The maximum impulse calculated from the modified Friedlander model is not significantly effected by the $R/(a/2)$.

- When only the displacement response is required, the Friedlander model may be used. However, if the acceleration response is of interest, the modified Friedlander model should be used.

- The nonlinear analysis provides a very good prediction of the plate subjected to air-blast load especially in the forced vibration zone.

- The linear analysis provides a good prediction of the plate subjected to air-blast load if the peak overpressure is low.

- For a rectangular plate, a square plate is the weakest configuration when subjected to air-blast load.

- An increase in the plate's area for a square plate increases the flexibility of the plate. However, the effect is reverse when the width of the plate is greater than 1 m for the loading considered.

- The effect of the charge location has on the response of the square plate subjected to air-blast loading is insignificant, provided that the projection of the charge location is on the plate's area.

6.2 Recommendation

This study was limited only on a low to medium magnitude air-blast. The effect of the temperature was not included. Only elastic response was considered in this study. It is, therefore, recommended that the following study should be considered:

- The plastic-elastic response should be incorporated in order that the model can be extended to study large magnitude air-blasts.
- The effect that a sudden temperature change has on the material properties of the plate and the response of the plate subjected to air-blast loading should be thoroughly investigated and incorporated in the analysis.

References

Abe,A., Kobayashi, Y., and Yamada, G., 1998, "Two-mode response of simply supported, rectangular laminated plates", International Journal of Non-Linear Mechanics, Vol. 33, No. 4, pp. 675-690.

Ambrosini, D., and Jacinto, A., 2005, "Numerical-experimental study of steel plates subjected to blast loading", WIT Transactions on Engineering Sciences, Vol. 49, pp. 49-62.

Chia, C.Y., 1980, Non-linear analysis of plates, McGraw-Hill, New York, USA.

Chung Kim Yuen, S., and Nurick, G. N., 2005. "Experimental and numerical studies on the response of quadrangular stiffened plates. Part I: subjected to uniform blast load", International Journal of Impact Engineering, 31, pp. 55-83.

Cichocki, K., and Perego, U., 1997, "Rectangular plates subjected to blast loading: the comparison between experimental results, numerical analysis and simplified analytical approach", Journal de physique. IV, Colloque, Vol. 7, No. 3, pp. 761-766.

Greenspan, D., 2006, Numerical solution of ordinary differential equations, WILEY-VCH Verlag GmbH and Co. KGaA, Weinheim.

Houlston, R., and DesRochers, C. G., 1987, "Nonlinear structural response of ship panels subjected to air blast loading", Computers & Structures, Vol.26, No. 1/2, pp.1-15.

Houlston, R., and Slater, J. E., 1987, "A summary of experimental results on square plates and stiffened panels subjected to air-blast loading", The Shock and Vibration Bulletin, 57, Part 2, pp. 55-67.

Houlston, R., Slater, J. E., Pegg, N., and DesRochers, C. G., 1985, "On analysis of structural response of ship panels subjected to air blast loading", Computers & Structures, Vol.21, No. 1/2, pp.273-289.

Hyde, D. W., 1991, "Conventional Weapons Effects program (ConWep)", US Army Engineer Waterways Experimental Station, Vicksburg, USA.

Jacinto, A. C., Ambrosini, R. D., and Danesi, R. F., 2001, "Experimental and computational analysis of plates under air blast loading", International Journal of Impact Engineering, 25, pp. 927-947.

Kinney, G. F., and Graham, K. J., 1985, "Explosive shocks in air", Second Edition, Springer-Verlag, New York, USA.

Lai, H. Y., Chen, C. K., and Yeh, Y. L., 2002, "Double-mode modeling of chaotic and bifurcation dynamics for a simply supported rectangular plate in large deflection", International Journal of Non-Linear Mechanics, 37, pp.331-343.

Lam, N., Mendis, P., and Ngo, T., 2004, "Response Spectrum Solutions for Blast Loading", Electronic Journal of Structural Engineering, 4, pp. 28-44.

Langdon, G. S., Chung Kim Yuen, S., and Nurick, G. N., 2005. "Experimental and numerical studies on the response of quadrangular stiffened plates. Part II: localised blast load", International Journal of Impact Engineering, 31, pp. 85-111.

Michael, M., and Swisdak, Jr., 2000, "BLAST EFFECTS COMPUTER (BEC)", from http://www.globalsecurity.org/military/library/report/2000/BECV4.xls.

Mosalam, K. M., and Mosallam, A. S., 2001, "Nonlinear transient analysis of reinforced concrete slabs subjected to blast loading and retrofitted with CFRP composites", Composites: Part B, 32, pp. 623-635.

Shu, X. F., Han, Q., and Yang, G. T., 1999, "The double mode model of the chaotic motion for a large deflection plate", Applied Mathematics and Mechanics, English Edition, Vol. 20, No. 4, pp. 360-364.

Smith, P. D., and Hetherington, J. G., 1994, "Blast and ballistic loading of structures" Published by Butterworth-Heinemann, Oxford, UK.

Taylor, R. L., and Govindjee, S., 2004, "Solution of clamped rectangular plate problem", Communication in Numerical Methods in Engineering, 20, pp. 757-765.

Teng, T. L., Liang, C. C., and Liao, C. C., 1996, "Transient dynamic large-deflection analysis of panel structure under blast loading", JSME International Journal, Series A, Vol. 39, No. 4, pp. 591-597.

Timoshenko, S., and Woinowsky-Krieger, S., 1959, Theory of plates and shells, McGraw-Hill, New York, USA.

Türkmen, H. S., 2002, "Structural response of laminated composite shells subjected to blast loading: comparison of experimental and theoretical methods", Journal of Sound and Vibration, 249(4), pp. 663-678.

Veldman, R. L., Ari-Gur, J., Clum, C., and DeYoung, A., and Folkert, J., 2006,

"Effects of pre-pressurization on blast response of clamped aluminum plates", International Journal of Impact Engineering, 32, pp. 1678-1695.

Woznica, K., Pennetier, O., and Renard, J., 2001, "Experiments and numerical simulations on thin metallic plates subjected to an explosion", Journal of Engineering Materials and Technology, Vol. 123, pp. 203-209.

Xue, Z. Y., and Hutchinson, J. W., 2003, "Preliminary assessment of sandwich plates subject to blast loads", International Journal of Mechanical Sciences, 45, pp. 687-705.

Zukas, J. A., and Walters, W. P., 1997, Explosive effects and applications, Springer-Verlag, New York, USA.

APPENDIX A

FUNCTION F_m

F_m in Eqn. (4.7) is explicitly expressed as:

$$F_1 = \frac{9Ea^2b^2w_{62}\left(w_{62}+w_{66}\right)}{2\left(36b^2+a^2\right)^2}, F_2 = \frac{Eb^2\left(w_{22}w_{26}+9w^2{}_{62}+w^2{}_{22}+9w_{62}w_{66}\right)}{2a^2},$$

$$F_3 = -\frac{Ea^2b^2\left(9w_{22}w_{66}+w_{22}w_{26}+25w_{26}w_{62}\right)}{16\left(b^2+4a^2\right)^2}, F_4 = -\frac{Ea^2b^2\left(w_{22}w_{62}+4w_{26}w_{62}+w_{22}w_{26}\right)}{4\left(b^2+a^2\right)^2},$$

$$F_5 = \frac{9Ea^2b^2\left(9w_{26}w_{62}+w_{22}w_{66}+10w_{26}w_{66}\right)}{2\left(16b^2+9a^2\right)^2}, F_6 = -\frac{Ea^2\left(w_{22}w_{62}+9w_{26}w_{66}\right)}{64b^2},$$

$$F_7 = \frac{9Ea^2b^2\left(10w_{62}w_{66}+9w_{26}w_{62}+w_{22}w_{66}\right)}{2\left(9b^2+16a^2\right)^2},$$

$$F_8 = \frac{9Ea^2b^2\left(w_{22}w_{62}+w_{62}{}^2+10w_{62}w_{66}+9w_{26}w_{62}+w_{22}w_{66}\right)}{2\left(9b^2+4a^2\right)^2}, F_9 = \frac{Ea^2b^2w_{66}\left(w_{26}+w_{66}\right)}{2\left(b^2+4a^2\right)^2},$$

$$F_{10} = -\frac{Ea^2b^2\left(w_{22}w_{62}+25w_{26}w_{62}+9w_{22}w_{66}\right)}{16\left(4b^2+a^2\right)^2}, F_{11} = -\frac{Ea^2b^2w_{26}w_{62}}{16\left(b^2+a^2\right)^2},$$

$$F_{12} = \frac{Ea^2\left(9w^2{}_{26}+9w_{26}w_{66}+w_{22}w_{62}+w^2{}_{22}\right)}{2b^2}, F_{13} = -\frac{9Ea^2b^2\left(w_{62}+w_{66}\right)\left(w_{22}+w_{62}\right)}{\left(9b^2+a^2\right)^2},$$

$$F_{14} = \frac{Ea^2b^2\left(w_{26}w_{62}+10w_{22}w_{62}+9w_{22}w_{66}\right)}{2\left(16b^2+a^2\right)^2}, F_{15} = -\frac{9Ea^2b^2\left(w_{26}+w_{66}\right)\left(w_{22}+w_{26}\right)}{\left(b^2+9a^2\right)^2},$$

$$F_{16} = \frac{Ea^2b^2\left(w_{26}w_{62}+10w_{22}w_{26}+9w_{22}w_{66}\right)}{2\left(b^2+16a^2\right)^2},$$

$$F_{17} = \frac{Ea^2b^2\left(w^2{}_{22}+9w_{22}w_{66}+w_{22}w_{62}+10w_{22}w_{26}+w_{26}w_{62}\right)}{2\left(b^2+4a^2\right)^2}, F_{18} = \frac{9Ea^2b^2w_{26}\left(w_{26}+w_{66}\right)}{2\left(b^2+36a^2\right)^2},$$

$$F_{19} = -\frac{Ea^2b^2\left(w_{22}+w_{26}\right)\left(w_{22}+w_{62}\right)}{\left(b^2+a^2\right)^2},$$

$$F_{20} = \frac{Ea^2b^2\left(w^2{}_{22}+9w_{22}w_{66}+10w_{22}w_{62}+w_{22}w_{26}+w_{22}w_{26}\right)}{2\left(4b^2+a^2\right)^2},$$

$$F_{21} = -\frac{Ea^2b^2\left(w_{62}+w_{66}\right)\left(w_{26}+w_{66}\right)}{\left(b^2+a^2\right)^2},$$

$$F_{22} = -\frac{Eb^2\left(w^2{}_{26}+9w^2{}_{66}\right)}{288a^2},$$

$$F_{23} = -\frac{Ea^2\left(w^2{}_{62}+9w^2{}_{66}\right)}{288b^2},$$

$$F_{24} = -\frac{9Ea^2b^2w_{66}w_{62}}{4\left(9b^2+a^2\right)^2},$$

$$F_{25} = \frac{Ea^2b^2w_{66}\left(w_{62}+w_{66}\right)}{2\left(4b^2+a^2\right)^2},$$

$$F_{26} = -\frac{Eb^2\left(w_{22}w_{26}+9w_{62}w_{66}\right)}{64a^2},$$

$$F_{27} = \frac{9Ea^2b^2\left(w^2{}_{26}+10w_{26}w_{66}+w_{22}w_{66}+9w_{26}w_{62}+w_{22}w_{26}\right)}{2\left(4b^2+9a^2\right)^2},$$

$$F_{28} = -\frac{9Ea^2b^2w_{66}w_{26}}{4\left(b^2+9a^2\right)^2},$$

$$F_{29} = -\frac{Eb^2\left(w^2{}_{22}+9w^2{}_{62}+18w_{62}w_{66}+2w_{22}w_{26}\right)}{32a^2},$$

$$F_{30} = -\frac{9Ea^2b^2w_{66}w_{62}}{16\left(9b^2+4a^2\right)^2},$$

$$F_{31} = -\frac{Ea^2\left(w^2{}_{22}+9w^2{}_{26}+18w_{26}w_{66}+2w_{22}w_{62}\right)}{32b^2},$$

$$F_{32} = \frac{Ea^2\left(w^2{}_{62}+9w^2{}_{66}+9w_{26}w_{66}+w_{22}w_{62}\right)}{18b^2},$$

$$F_{33} = \frac{Eb^2\left(9w^2{}_{66}+w^2{}_{26}+w_{22}w_{26}+9w_{62}w_{66}\right)}{18a^2},$$

$$F_{34} = -\frac{9Ea^2b^2w_{66}w_{26}}{16\left(4b^2+9a^2\right)^2}.$$

APPENDIX B

FUNCTION V_m

V_m in Eqn. (4.8) is explicitly expressed as:

$$V_1 = \frac{3E\pi^4(16\beta_1\lambda^4 - 33\lambda^4 - 32\alpha\lambda^4 - 33 + 16\alpha_1\lambda^4)}{25b^4\rho},$$

$$V_2 = \frac{3E\pi^4(216\gamma_1\lambda^4 + 38\alpha_1\lambda^4 - 41\lambda^4 + 12\beta_1\lambda^4 + 320\alpha_3\lambda^4 + 198 + 16\alpha\lambda^4 + 864\alpha_2\lambda^4)}{25b^4\rho},$$

$$V_3 = \frac{1}{25b^4\rho}3E\pi^4(-41 + 198\lambda^4 + 864\beta_2\lambda^4 + 16\alpha\lambda^4 + 320\beta_3\lambda^4 + 216\delta_1\lambda^4 + 12\alpha_1\lambda^4 + 38\beta_1\lambda^4),$$

$$V_4 = -\frac{1}{25b^4\rho}54E\pi^4(-48\alpha_2\lambda^4 - 9\lambda^4 - 12\gamma_1\lambda^4 - 48\beta_2\lambda^4 - 12\delta_1\lambda^4 - 16\beta_3\lambda^4 + 24\delta_2\lambda^4 - 16\alpha_3\lambda^4 + 24\gamma_2 2\lambda^4 + 3\beta_1\lambda^4 + 3\alpha_1\lambda^4 - 9),$$

$$V_5 = -\frac{1}{25b^4\rho}3E\pi^4(-432\alpha_2\lambda^4 - 64\alpha\lambda^4 - 2052\gamma_1\lambda^4 + 12\lambda^4 + 1120\alpha_3\lambda^4 + 4\beta_1\lambda^4 + 1073\alpha_1\lambda^4 + 297),$$

$$V_6 = -\frac{1}{25b^4\rho}3E\pi^4(1073\beta_1\lambda^4 + 12 - 2052\delta_1\lambda^4 + 4\alpha_1\lambda^4 - 64\alpha\lambda^4 + 1120\beta_3\lambda^4 - 432\beta_2\lambda^4 + 297\lambda^4),$$

$$V_7 = -\frac{1}{25b^4\rho}27E\pi^4(-16\lambda^4 - 612\gamma_2\lambda^4 - 612\gamma_1\lambda^4 + 144\beta_2\lambda^4 - 16 - 612\delta_1\lambda^4 + 135\alpha_1\lambda^4 + 144\alpha_2\lambda^4 + 135\beta_1\lambda^4 + 108\alpha_3\lambda^4 - 612\delta_2\lambda^4 + 108\beta_3\lambda^4),$$

$$V_8 = -\frac{1}{25b^4\rho}12E\pi^4(84\beta_1\lambda^4 - 88\alpha\lambda^4 + 84\alpha_1\lambda^4 - 28\alpha_3\lambda^4 - 1944\gamma_1\lambda^4 - 21\lambda^4 - 28\beta_3\lambda^4 - 1944\delta_1\lambda^4 - 21 + 972\gamma_2\lambda^4 + 972\delta_2\lambda^4),$$

$$V_9 = \frac{1}{25b^4\rho}18E\pi^4(24\lambda^4 - 468\delta_2\lambda^4 + 972\gamma_2\lambda^4 + 1584\gamma_1\lambda^4 - 144\alpha_2\lambda^4 - 282\alpha_1\lambda^4 - 348\alpha_3\lambda^4 - 21 + 12\beta_3\lambda^4 + 972\delta_1\lambda^4 + 51\beta_1\lambda^4),$$

$$V_{10} = -\frac{1}{25b^4\rho}18E\pi^4(144\beta_2\lambda^4 - 972\delta_2\lambda^4 + 282\beta_1\lambda^4 - 972\gamma_1\lambda^4 + 21\lambda^4 - 1584\delta_1\lambda^4 - 12\alpha_3\lambda^4 + 348\beta_3\lambda^4 + 468\gamma_2\lambda^4 - 28 - 51\alpha_1\lambda^4),$$

$$V_{11} = \frac{4\pi^4H^2E(5 + 5\lambda^4 + 6\lambda^2)}{25\rho(-1+\upsilon)(\upsilon+1)b^4},$$

$$V_{12} = \frac{6E\pi^4(918\gamma_1\lambda^4 + 891 + 432\alpha_4\lambda^4 + 5\lambda^4 - 216\alpha_2\lambda^4)}{25b^4\rho},$$

$$V_{13}=\frac{1}{25b^4\rho}3E\pi^4(-96\lambda^4+1246\beta_1\lambda^4+52488\gamma_2\lambda^4+13608\delta_2\lambda^4-243-112\alpha_3\lambda^4$$
$$+1063\alpha_1\lambda^4+8\beta_3\lambda^4+52488\delta_1\lambda^4+22356\gamma_1\lambda^4+1200\alpha\lambda^4),$$
$$V_{14}=-\frac{1}{25b^4\rho}18E\pi^4(-252\alpha_4\lambda^4+576\alpha_2\lambda^4-144\alpha\gamma^4+10\lambda^4+72\alpha_1\lambda^4-2520\delta_2\lambda^4$$
$$-3960\gamma_1\lambda^4-369),$$
$$V_{15}=\frac{1}{25b^4\rho}3E\pi^4(1063\beta_1\lambda^4+1200\alpha\lambda^4-112\beta_3\lambda^4+1246\alpha_1\lambda^4+8\alpha_3\lambda^4-243\lambda^4-96$$
$$+13608\gamma_2\lambda^4+52488\gamma_1\lambda^4+52488\delta_2\lambda^4+22356\delta_1\lambda^4),$$
$$V_{16}=-\frac{54E\pi^4(36\alpha_1\lambda^4-5\lambda^4-3069\gamma_1\lambda^4-144\alpha\lambda^4-36\alpha_4\lambda^4-3060\delta_2\lambda^4-72\alpha_2\lambda^4-36)}{25b^4\rho},$$
$$V_{17}=-\frac{1}{25b^4\rho}27E\pi^4(-11988\gamma_2\lambda^4+87\alpha_1\lambda^4+87\beta_1\lambda^4-11988\delta_2\lambda^4+28-11988\delta_1\lambda^4$$
$$-384\alpha\lambda^4-11988\gamma_1\lambda^4+28\lambda^4+12\beta_3\lambda^4+12\alpha_3\lambda^4),$$
$$V_{18}=\frac{72\pi^4H^2E(15+2\lambda^2)}{25\rho(-1+\upsilon)(\upsilon+1)b^4},$$
$$V_{19}=\frac{6E\pi^4(891\lambda^4-216\beta_2\lambda^4+5+918\delta_1\lambda^4+432\beta_4\lambda^4)}{25b^4\rho},$$
$$V_{20}=-\frac{1}{25b^4\rho}18E\pi^4(-369\lambda^4-144\alpha\lambda^4+10-3960\delta_1\lambda^4+576\beta_2\lambda^4-252\beta_4\lambda^4$$
$$+72\beta_1\lambda^4-2520\gamma_2\lambda^4),$$
$$V_{21}=-\frac{54E\pi^4}{25b^4\rho}(-36\beta_4\lambda^4+36\beta_1\lambda^4-3069\gamma_1\lambda^4-144\alpha\lambda^4-36\alpha_4\lambda^4-3060\delta_2\lambda^4$$
$$-72\alpha_2\lambda^4-36),$$
$$V_{22}=-\frac{72\pi^4H^2E\lambda^2(15\lambda^2+2)}{25\rho(-1+\upsilon)(\upsilon+1)b^4},$$
$$V_{23}=-\frac{324E\pi^4(-16\alpha\lambda^4+2\alpha_1\lambda^4+5+5\lambda^4+2\beta_1\lambda^4)}{25b^4\rho},$$
$$V_{24}=\frac{864\pi^4H^2E\lambda^2}{25\rho(-1+\upsilon)(\upsilon+1)b^4},$$
$$V_{25}=-\frac{\mu}{H\rho},$$
$$V_{26}=\frac{4}{25H\rho},$$
$$V_{27}=-\frac{E\pi^4(-68\beta_1\lambda^4+112\alpha_1\lambda^4+16\alpha\lambda^4-66-21\lambda^4)}{25b^4\rho},$$
$$V_{28}=-\frac{E\pi^4(192\alpha\lambda^4+851\alpha_1\lambda^4+1440\alpha_3\lambda^4+972\gamma_1\lambda^4-76\beta_1\lambda^4+18\lambda^4+3888\alpha_2\lambda^4+891)}{25b^4\rho},$$

$$V_{29}=-\frac{2E\pi^4}{25b^4\rho}(-1296\beta_2\lambda^4-467\beta_1\lambda^4-324\delta_1\lambda^4-41+62\alpha_1\lambda^4+136\alpha\lambda^4+63\lambda^4$$
$$-280\beta_3\lambda^4),$$
$$V_{30}=-\frac{1}{25b^4\rho}9E\pi^4(-56\beta_3\lambda^4-216\gamma_2\lambda^4+81+43\alpha_1\lambda^4+432\alpha_2\lambda^4-142\beta_1\lambda^4+144\alpha_3\lambda^4$$
$$+36\lambda^4-72\delta_1\lambda^4+108\gamma_1\lambda^4-216\delta_2\lambda^4-288\beta_2\lambda^4),$$
$$V_{31}=-\frac{2E\pi^4}{25b^4\rho}(-1073\alpha_1\lambda^4+5832\alpha_2\lambda^4-297+48\lambda^4-1458\gamma_1\lambda^4-4\beta_1\lambda^4+64\alpha\lambda^4$$
$$-1120\alpha_3\lambda^4),$$
$$V_{32}=-\frac{3E\pi^4(-63\lambda^4-2592\beta_2\lambda^4-8+2268\delta_1\lambda^4-680\beta_3\lambda^4-607\beta_1\lambda^4+4\alpha_1\lambda^4+176\alpha\lambda^4)}{25b^4\rho},$$
$$V_{33}=\frac{1}{25b^4\rho}18E\pi^4(135\alpha_1\lambda^4+108\beta_3\lambda^4-1512\delta_2\lambda^4-612\gamma_2\lambda^4-612\delta_1\lambda^4-216\alpha_2\lambda^4$$
$$-1512\gamma_1\lambda^4-16+135\beta_1\lambda^4+108\alpha_3\lambda^4+144\beta_2\lambda^4-36\lambda^4),$$
$$V_{34}=-\frac{1}{25b^4\rho}2E\pi^4(189+252\alpha_3\lambda^4-751\beta_1\lambda^4+17496\gamma_1\lambda^4-8748\gamma_2\lambda^4-446\alpha_1\lambda^4$$
$$+752\alpha\lambda^4+2916\delta_1\lambda^4-8748\delta_2\lambda^4-216\lambda^4+52\beta_3\lambda^4),$$
$$V_{35}=\frac{1}{25b^4\rho}36E\pi^4(-324\gamma_2\lambda^4-17\beta_1\lambda^4+7+4\lambda^4-324\delta_1\lambda^4+756\delta_2\lambda^4+94\alpha_1\lambda^4$$
$$+116\alpha_3\lambda^4-918\gamma_1\lambda^4-432\alpha_2\lambda^4-4\beta_3\lambda^4),$$
$$V_{36}=-\frac{1}{25b^4\rho}27E\pi^4(-384\beta_2\lambda^4+71\alpha_1\lambda^4-77\beta_1\lambda^4-468\gamma_2\lambda^4+444\delta_1\lambda^4+24\lambda^4$$
$$+28+12\alpha_3\lambda^4-148\beta_3\lambda^4+972\gamma_1\lambda^4+972\delta_2\lambda^4),$$
$$V_{37}=-\frac{8EH^2\pi^4(6\lambda^2+5)}{75\rho(-1+\upsilon)(\upsilon+1)b^4},$$
$$V_{38}=-\frac{3E\pi^4(35\lambda^4+2592\alpha_2\lambda^4+2673-1296\gamma_1\lambda^4+1296\alpha_4\lambda^4)}{25b^4\rho},$$
$$V_{39}=\frac{1}{25b^4\rho}2E\pi^4(-52488\gamma_2\lambda^4+960\alpha\lambda^4-1063\alpha_1\lambda^4+34992\delta_2\lambda^4-52488\delta_1\lambda^4$$
$$+4374\gamma_1\lambda^4-8\beta_3\lambda^4-1246\beta_1\lambda^4+243+112\alpha_3\lambda^4+216\lambda^4),$$
$$V_{40}=\frac{1}{25b^4\rho}9E\pi^4(1350\gamma_1\lambda^4+70\lambda^4-1170+8640\delta_2\lambda^4-432\alpha_2\lambda^4+288\alpha\lambda^4$$
$$-756\alpha_4\lambda^4+216\alpha_1\lambda^4),$$
$$V_{41}=-\frac{1}{25b^4\rho}3E\pi^4(-162\lambda^4-144-68\beta_3\lambda^4+1757\beta_1\lambda^4+78732\delta_2\lambda^4+20412\gamma_2\lambda^4$$
$$+2000\alpha\lambda^4+12\alpha_3\lambda^4+1879\alpha_1\lambda^4+78732\gamma_1\lambda^4+26244\delta_1\lambda^4),$$
$$V_{42}=\frac{1}{25b^4\rho}27E\pi^4(-35\lambda^4-108-10080\delta_2\lambda^4+48\alpha\lambda^4-108\alpha_4\lambda^4+108\alpha_1\lambda^4$$
$$-576\alpha_2\lambda^4-10107\gamma_1\lambda^4),$$

$$V_{43}=-\frac{1}{25b^4\rho}18E\pi^4(-87\alpha_1\lambda^4+11988\delta_1\lambda^4+28188\gamma_1\lambda^4+144\alpha\lambda^4-28-12\alpha_3\lambda^4$$
$$+28188\delta_2\lambda^4+12\lambda^4+11988\gamma_2\lambda^4-87\beta_1\lambda^4-12\beta_3\lambda^4),$$
$$V_{44}=\frac{4\pi^2H^2E(5\lambda^4+54\lambda^2+405)}{25\rho(-1+\upsilon)(\upsilon+1)b^4},$$
$$V_{45}=\frac{2E\pi^4(-3726\delta_1\lambda^4-567\lambda^4+2592\beta_2\lambda^4-324\beta_4\lambda^4-10)}{25b^4\rho},$$
$$V_{46}=-\frac{54E\pi^4(-288\beta_2\lambda^4+1260\gamma_2\lambda^4-18\lambda^4-5+1575\delta_1\lambda^4+36\beta_4\lambda^4-36\beta_1\lambda^4+72\alpha\lambda^4)}{25b^4\rho},$$
$$V_{47}=-\frac{36E\pi^4(72\beta_2\lambda^4+144\alpha\lambda^4+3060\gamma_2\lambda^4+3069\delta_1\lambda^4-144\lambda^4+5-126\beta_1\lambda^4+36\beta_4\lambda^4)}{25b^4\rho},$$
$$V_{48}=\frac{96\pi^4H^2E\lambda^2}{25\rho(-1+\upsilon)(\upsilon+1)b^4},$$
$$V_{49}=-\frac{162E\pi^4(8\alpha\lambda^4-6\alpha_1\lambda^4-35\lambda^4-16\beta_1\lambda^4-15)}{25b^4\rho},$$
$$V_{50}=-\frac{216\pi^4H^2E\lambda^2(5\lambda^2+6)}{25\rho(-1+\upsilon)(\upsilon+1)b^4},$$
$$V_{51}=-\frac{\mu}{H\rho},$$
$$V_{52}=\frac{4}{25H\rho},$$
$$V_{53}=-\frac{E\pi^4(-66\lambda^4-21-68\alpha_1\lambda^4+16\alpha\lambda^4+112\beta_1\lambda^4)}{25b^4\rho},$$
$$V_{54}=-\frac{2E\pi^4(-41\lambda^4+63+62\beta_1\lambda^4+136\alpha\lambda^4-324\gamma_1\lambda^4-467\alpha_1\lambda^4-1296\alpha_2\lambda^4-280\alpha_3\lambda^4)}{25b^4\rho},$$
$$V_{55}=-\frac{E\pi^4(3888\beta_2\lambda^4+851\beta_1\lambda^4-76\alpha_1\lambda^4+192\alpha\lambda^4+1440\beta_3\lambda^4+891\lambda^4+972\delta_1\lambda^4+18)}{25b^4\rho},$$
$$V_{56}=\frac{1}{25b^4\rho}9E\pi^4(-144\beta_3\lambda^4+216\gamma_2\lambda^4+142\alpha_1\lambda^4-36-108\delta_1\lambda^4+216\delta_2\lambda^4-432\beta_2\lambda^4$$
$$+72\gamma_1\lambda^4-43\beta_1\lambda^4+288\alpha_2\lambda^4-81\lambda^4+56\alpha_3\lambda^4),$$
$$V_{57}=-\frac{3E\pi^4(-8\lambda^4-63+4\beta_1\lambda^4+176\alpha\lambda^4+2268\gamma_1\lambda^4-607\alpha_1\lambda^4-2592\alpha_2\lambda^4-680\alpha_3\lambda^4)}{25b^4\rho},$$
$$V_{58}=-\frac{2E\pi^4(5832\beta_2\lambda^4-1073\beta_1\lambda^4+64\alpha\lambda^4-1458\delta_1\lambda^4-4\alpha_1\lambda^4+48-1120\beta_3\lambda^4-297\lambda^4)}{25b^4\rho},$$
$$V_{59}=\frac{1}{25b^4\rho}18E\pi^4(-36+108\beta_3\lambda^4+135\beta_1\lambda^4-1512\delta_1\lambda^4-612\delta_2\lambda^4-1512\gamma_2\lambda^4-16\lambda^4$$
$$+135\alpha_1\lambda^4-216\beta_2\lambda^4+108\alpha_3\lambda^4+144\alpha_2\lambda^4-612\gamma_1\lambda^4),$$

$$V_{60}=-\frac{1}{25b^4\rho}2E\pi^4(-216+189\lambda^4+752\alpha\lambda^4-446\beta_1\lambda^4+52\alpha_3\lambda^4-751\alpha_1\lambda^4$$
$$+252\beta_3\lambda^4+17496\delta_1\lambda^4+2916\gamma_1\lambda^4-8748\gamma_2\lambda^4-8748\delta_2\lambda^4),$$
$$V_{61}=\frac{1}{25b^4\rho}27E\pi^4(77\alpha_1\lambda^4-972\gamma_2\lambda^4-972\delta_1\lambda^4-24+468\delta_2\lambda^4-12\beta_3\lambda^4$$
$$-444\gamma_1\lambda^4-71\beta_1\lambda^4+384\alpha_2\lambda^4-28\lambda^4+148\alpha_3\lambda^4),$$
$$V_{62}=-\frac{1}{25b^4\rho}36E\pi^4(-7\lambda^4-116\beta_3\lambda^4-756\gamma_2\lambda^4+17\alpha_1\lambda^4-4+918\delta_1\lambda^4$$
$$+324\delta_2\lambda^4+432\beta_2\lambda^4+324\gamma_1\lambda^4-94\beta_1\lambda^4+4\alpha_3\lambda^4),$$
$$V_{63}=-\frac{8\pi^4H^2E\lambda^2(6+5\lambda^2)}{75\rho(-1+\upsilon)(\upsilon+1)b^4},$$
$$V_{64}=\frac{2E\pi^4(-567-324\alpha_4\lambda^4+2592\alpha_2\lambda^4-10\lambda^4-3726\gamma_1\lambda^4)}{25b^4\rho},$$
$$V_{65}=-\frac{1}{25b^4\rho}3E\pi^4(-162-144\lambda^4+2000\alpha\lambda^4+1879\beta_1\lambda^4-68\alpha_3\lambda^4+1757\alpha_1\lambda^4$$
$$+12\beta_3\lambda^4+78732\delta_1\lambda^4+26244\gamma_1\lambda^4+78732\gamma_2\lambda^4+20412\delta_2\lambda^4),$$
$$V_{66}=-\frac{54E\pi^4}{25b^4\rho}(-18+36\alpha_4\lambda^4+72\alpha\lambda^4+1260\delta_2\lambda^4-36\alpha_1\lambda^4-288\alpha_2\lambda^4+1575\gamma_1\lambda^4-5\lambda^4),$$
$$V_{67}=\frac{1}{25b^4\rho}2E\pi^4(216+243\lambda^4+960\alpha\lambda^4-1063\beta_1\lambda^4-8\alpha_3\lambda^4-1246\alpha_1\lambda^4$$
$$+112\beta_3\lambda^4+4374\delta_1\lambda^4-52488\gamma_1\lambda^4+34992\gamma_2\lambda^4-52488\delta_2\lambda^4),$$
$$V_{68}=-\frac{1}{25b^4\rho}36E\pi^4(-126\alpha_1\lambda^4+144\alpha\lambda^4-144+3060\delta_2\lambda^4+3069\gamma_1\lambda^4+36\alpha_4\lambda^4$$
$$+72\alpha_2\lambda^4+5\lambda^4),$$
$$V_{69}=-\frac{1}{25b^4\rho}18E\pi^4(-12\beta_3\lambda^4+11988\gamma_1\lambda^4-28\lambda^4-12\alpha_3\lambda^4-87\alpha_1\lambda^4+28188\gamma_2\lambda^4$$
$$+28188\delta_1\lambda^4+12-87\beta_1\lambda^4+11988\delta_2\lambda^4+144\alpha\lambda^4),$$
$$V_{70}=\frac{96\pi^4H^2E\lambda^2}{25\rho(-1+\upsilon)(\upsilon+1)b^4},$$
$$V_{71}=-\frac{3E\pi^4(1296\beta_4\lambda^4+2592\beta_2\lambda^4+2673\lambda^4-1296\delta_1\lambda^4+35)}{25b^4\rho},$$
$$V_{72}=\frac{1}{25b^4\rho}9E\pi^4(-756\beta_4\lambda^4-1107\lambda^4-432\beta_2\lambda^4+1350\delta_1\lambda^4+8640\gamma_2\lambda^4+70$$
$$+216\beta_1\lambda^4+288\alpha\lambda^4),$$
$$V_{73}=\frac{1}{25b^4\rho}27E\pi^4(108\beta_1\lambda^4-576\beta_2\lambda^4+48\alpha\lambda^4-35-10080\gamma_2\lambda^4-108\beta_4\lambda^4$$
$$-108\lambda^4-10107\delta_1\lambda^4),$$

$$V_{74}=\frac{4\pi^4H^2E(54\lambda^2+405\lambda^4+5)}{25\rho(-1+\upsilon)(\upsilon+1)b^4},$$

$$V_{75}=-\frac{162E\pi^4(-6\beta_1\lambda^4-35-16\alpha_1\lambda^4+8\alpha\lambda^4-15\lambda^4)}{25b^4\rho},$$

$$V_{76}=-\frac{216\pi^4H^2E(5+6\lambda^2)}{25\rho(-1+\upsilon)(\upsilon+1)b^4},$$

$$V_{77}=-\frac{\mu}{H\rho},$$

$$V_{78}=\frac{4}{25H\rho},$$

$$V_{79}=\frac{-2E\pi^4(7-32\alpha\lambda^4+46\alpha_1\lambda^4+46\beta_1\lambda^4+7\lambda^4)}{25b^4\rho},$$

$$V_{80}=-\frac{3E\pi^4(-4\lambda^4-96\alpha\lambda^4+1296\alpha_2\lambda^4+324\gamma_1\lambda^4-63+28\beta_1\lambda^4+280\alpha_3\lambda^4+377\alpha_1\lambda^4)}{25b^4\rho},$$

$$V_{81}=-\frac{3E\pi^4(-63\lambda^4-96\alpha\lambda^4+324\delta_1\lambda^4+280\beta_3\lambda^4+28\alpha_1\lambda^4-4+1296\beta_2\lambda^4+377\beta_1\lambda^4)}{25b^4\rho},$$

$$V_{82}=-\frac{1}{25b^4\rho}27E\pi^4(108\delta_2\lambda^4-18+144\alpha_2\lambda^4+36\delta_1\lambda^4+61\beta_1\lambda^4+28\alpha_3\lambda^4+36\gamma_1\lambda^4,$$
$$+61\alpha_1\lambda^4+108\gamma_2\lambda^4+144\beta_2\lambda^4-18\lambda^4+28\beta_3\lambda^4),$$

$$V_{83}=-\frac{2E\pi^4(-32\lambda^4+5022\gamma_1\lambda^4+2592\alpha_2\lambda^4+680\alpha_3\lambda^4+607\alpha_1\lambda^4-176\alpha\lambda^4-4\beta_1\lambda^4+63)}{25b^4\rho},$$

$$V_{84}=\frac{2E\pi^4(4\alpha_1\lambda^4-2592\beta_2\lambda^4-607\beta_1\lambda^4-63\lambda^4+176\alpha\lambda^4-5022\delta_1\lambda^4+32-680\beta_3\lambda^4)}{25b^4\rho},$$

$$V_{85}=-\frac{1}{25b^4\rho}108E\pi^4(12\alpha_3\lambda^4-168\gamma_2\lambda^4+15\beta_1\lambda^4-4\lambda^4+12\beta_3\lambda^4-24\alpha_2\lambda^4-24\beta_2\lambda^4$$
$$+15\alpha_1\lambda^4-168\delta_2\lambda^4-168\gamma_1\lambda^4-4-168\delta_1\lambda^4),$$

$$V_{86}=-\frac{1}{25b^4\rho}E\pi^4(648+1873\beta_1\lambda^4+26244\gamma_2\lambda^4+26244\delta_2\lambda^4-8748\gamma_1\lambda^4+648\lambda^4$$
$$-156\alpha_3\lambda^4-156\beta_3\lambda^4-8748\delta_1\lambda^4+1873\alpha_1\lambda^4-1536\alpha\lambda^4),$$

$$V_{87}=-\frac{1}{25b^4\rho}18E\pi^4(2268\delta_2\lambda^4+148\alpha_3\lambda^4+77\alpha_1\lambda^4+144\alpha_2\lambda^4-24-71\beta_1\lambda^4+12\lambda^4$$
$$-972\gamma_2\lambda^4-972\delta_1\lambda^4+36\gamma_1\lambda^4-12\beta_3\lambda^4),$$

$$V_{88}=\frac{1}{25b^4\rho}18E\pi^4(972\delta_2\lambda^4-148\beta_3\lambda^4-12+71\alpha_1\lambda^4-2268\gamma_2\lambda^4-77\beta_1\lambda^4+972\gamma_1\lambda^4$$
$$-36\delta_1\lambda^4+12\alpha_3\lambda^4-144\beta_2\lambda^4+24\lambda^4),$$

$$V_{89}=\frac{32\pi^4H^2E\lambda^2}{75\rho(-1+\upsilon)(\upsilon+1)b^4},$$

$$V_{90} = -\frac{E\pi^4(-972\alpha_4\lambda^4 - 1701 - 70\lambda^4 + 9072\gamma_1\lambda^4 + 1296\alpha_2\lambda^4)}{25b^4\rho},$$

$$V_{91} = \frac{1}{25b^4\rho}2E\pi^4(-162 - 52488\delta_2\lambda^4 + 78732\gamma_2\lambda^4 - 1240\alpha\lambda^4 + 1757\alpha_1\lambda^4 + 1879\beta_1\lambda^4 - 324\lambda^4 + 12\beta_3\lambda^4 - 68\alpha_3\lambda^4 + 78732\delta_1\lambda^4 - 32076\gamma_1\lambda^4),$$

$$V_{92} = -\frac{1}{25b^4\rho}27E\pi^4(384\alpha_2\lambda^4 - 108\alpha_4\lambda^4 + 108\alpha_1\lambda^4 + 2715\gamma_1\lambda^4 + 54 + 35\lambda^4 + 4320\delta_2\lambda^4 + 144\alpha\lambda^4),$$

$$V_{93} = \frac{1}{25b^4\rho}2E\pi^4(-1240\alpha\lambda^4 + 78732\delta_2\lambda^4 + 78732\gamma_1\lambda^4 + 12\alpha_3\lambda^4 + 1757\beta_1\lambda^4 + 68\beta_3\lambda^4 - 32076\delta_1\lambda^4 - 52488\gamma_2\lambda^4 - 324 + 1879\alpha_1\lambda^4 - 162\lambda^4),$$

$$V_{94} = -\frac{1}{25b^4\rho}18E\pi^4(378\alpha_1\lambda^4 - 108\alpha_4\lambda^4 + 648\alpha\lambda^4 - 10080\delta_2\lambda^4 + 432 - 35\lambda^4 - 10107\gamma_1\lambda^4 - 576\alpha_2\lambda^4),$$

$$V_{95} = -\frac{1}{25b^4\rho}36E\pi^4(29\beta_1\lambda^4 - 9396\gamma_1\lambda^4 - 9396\delta_2\lambda^4 - 9396\delta_1\lambda^4 + 4\beta_3\lambda^4 + 4\alpha_3\lambda^4 + 29\alpha_1\lambda^4 + 432\alpha\lambda^4 - 4\lambda^4 - 9396\gamma_2\lambda^4 - 4),$$

$$V_{96} = -\frac{8\pi^4H^2E\lambda^2(5\lambda^2 + 54)}{75\rho(-1+\upsilon)(\upsilon+1)b^4},$$

$$V_{97} = -\frac{E\pi^4(-1701\lambda^4 + 9072\delta_1\lambda^4 + 1296\beta_2\lambda^4 - 972\beta_4\lambda^4 - 70)}{25b^4\rho},$$

$$V_{98} = -\frac{1}{25b^4\rho}27E\pi^4(54\lambda^4 - 108\beta_4\lambda^4 + 4320\gamma_2\lambda^4 + 35 + 384\beta_2\lambda^4 + 144\alpha\lambda^4 + 108\beta_1\lambda^4 + 2715\delta_1\lambda^4),$$

$$V_{99} = -\frac{1}{25b^4\rho}18E\pi^4(378\beta_1\lambda^4 - 10107\delta_1\lambda^4 - 35 - 576\beta_2\lambda^4 + 432\lambda^4 - 10080\gamma_2\lambda^4 - 108\beta_4\lambda^4 + 648\alpha\lambda^4),$$

$$V_{100} = -\frac{8EH^2\pi^4(54\lambda^2 + 5)}{75\rho(-1+\upsilon)(\upsilon+1)b^4},$$

$$V_{101} = -\frac{243E\pi^4(35\lambda^4 + 35 + 16\beta_1\lambda^4 + 16\alpha_1\lambda^4 + 32\alpha\lambda^4)}{25b^4\rho},$$

$$V_{102} = \frac{324EH^2\pi^4(5 + 6\lambda^2 + 5\lambda^4)}{25\rho(-1+\upsilon)(\upsilon+1)b^4},$$

$$V_{103} = -\frac{\mu}{H\rho},$$

$$V_{104} = \frac{4}{25H\rho}.$$

where

$$\lambda = \frac{b}{a},$$

$$\alpha = \frac{1}{(\lambda^2+1)^2}, \alpha_1 = \frac{1}{(\lambda^2+4)^2}, \alpha_2 = \frac{1}{(\lambda^2+9)^2}, \alpha_3 = \frac{1}{(\lambda^2+16)^2}, \alpha_4 = \frac{1}{(36+\lambda^2)^2},$$

$$\beta_1 = \frac{1}{(4\lambda^2+1)^2}, \beta_2 = \frac{1}{(9\lambda^2+1)^2}, \beta_3 = \frac{1}{(1+16\lambda^2)^2}, \beta_4 = \frac{1}{(1+36\lambda^2)^2},$$

$$\gamma_1 = \frac{1}{(9+4\lambda^2)^2}, \gamma_2 = \frac{1}{(9\lambda^2+16)^2},$$

$$\delta_1 = \frac{1}{(9\lambda^2+4)^2}, \delta_2 = \frac{1}{(9+16\lambda^2)^2}.$$

APPENDIX C

FUNCTION P_m

P_m in Eqns. (4.8) and (4.9) is explicitly expressed as:

$$
\begin{aligned}
P_1 = 9\int_A [p(x,y,t)]\times\left(1-\cos\frac{2\pi x}{a}\right)\left(1-\cos\frac{2\pi y}{b}\right)dA \\
-6\int_A [p(x,y,t)]\times\left(1-\cos\frac{2\pi x}{a}\right)\left(1-\cos\frac{6\pi y}{b}\right)dA \\
-6\int_A [p(x,y,t)]\times\left(1-\cos\frac{6\pi x}{a}\right)\left(1-\cos\frac{2\pi y}{b}\right)dA \\
+4\int_A [p(x,y,t)]\times\left(1-\cos\frac{6\pi x}{a}\right)\left(1-\cos\frac{6\pi y}{b}\right)dA \\
P_2 = -6\int_A [p(x,y,t)]\times\left(1-\cos\frac{2\pi x}{a}\right)\left(1-\cos\frac{2\pi y}{b}\right)dA \\
+9\int_A [p(x,y,t)]\times\left(1-\cos\frac{2\pi x}{a}\right)\left(1-\cos\frac{6\pi y}{b}\right)dA \\
+4\int_A [p(x,y,t)]\times\left(1-\cos\frac{6\pi x}{a}\right)\left(1-\cos\frac{2\pi y}{b}\right)dA \\
-6\int_A [p(x,y,t)]\times\left(1-\cos\frac{6\pi x}{a}\right)\left(1-\cos\frac{6\pi y}{b}\right)dA \\
P_3 = -6\int_A [p(x,y,t)]\times\left(1-\cos\frac{2\pi x}{a}\right)\left(1-\cos\frac{2\pi y}{b}\right)dA \\
+4\int_A [p(x,y,t)]\times\left(1-\cos\frac{2\pi x}{a}\right)\left(1-\cos\frac{6\pi y}{b}\right)dA \\
+9\int_A [p(x,y,t)]\times\left(1-\cos\frac{6\pi x}{a}\right)\left(1-\cos\frac{2\pi y}{b}\right)dA \\
-6\int_A [p(x,y,t)]\times\left(1-\cos\frac{6\pi x}{a}\right)\left(1-\cos\frac{6\pi y}{b}\right)dA \\
P_4 = 4\int_A [p(x,y,t)]\times\left(1-\cos\frac{2\pi x}{a}\right)\left(1-\cos\frac{2\pi y}{b}\right)dA \\
-6\int_A [p(x,y,t)]\times\left(1-\cos\frac{2\pi x}{a}\right)\left(1-\cos\frac{6\pi y}{b}\right)dA \\
-6\int_A [p(x,y,t)]\times\left(1-\cos\frac{6\pi x}{a}\right)\left(1-\cos\frac{2\pi y}{b}\right)dA \\
+9\int_A [p(x,y,t)]\times\left(1-\cos\frac{6\pi x}{a}\right)\left(1-\cos\frac{6\pi y}{b}\right)dA
\end{aligned}
$$

APPENDIX D

FUNCTION J_m

J_m in Eqn. (4.9) is explicitly expressed as:

$$J_1 = \frac{(24\pi^4 H^3 E a^2 b^2 + 20\pi^4 H^3 E a^4 + 20\pi^4 H^3 E b^4)}{25\rho H a^4 b^4 (\upsilon^2 - 1)},$$

$$J_2 = \frac{(-144\pi^4 H^3 E a^2 b^2 - 1080\pi^4 H^3 E a^4)}{25\rho H a^4 b^4 (\upsilon^2 - 1)},$$

$$J_3 = \frac{(-1080\pi^4 H^3 E b^4 - 144\pi^4 H^3 E a^2 b^2)}{25\rho H a^4 b^4 (\upsilon^2 - 1)}, \quad J_4 = \frac{864\pi^4 H^2 E}{25 a^2 b^2 \rho (\upsilon^2 - 1)},$$

$$J_5 = \frac{\mu}{H\rho}, \quad J_6 = \frac{4}{25baH\rho},$$

$$J_7 = -\frac{(40\pi^4 H^3 E a^4 + 48\pi^4 H^3 E a^2 b^2)}{75\rho H a^4 b^4 (\upsilon^2 - 1)},$$

$$J_8 = -\frac{(-648\pi^4 H^3 E a^2 b^2 - 60\pi^4 H^3 E b^4 - 4860\pi^4 H^3 E a^4)}{75\rho H a^4 b^4 (\upsilon^2 - 1)},$$

$$J_9 = \frac{96\pi^4 H^2 E}{25 a^2 b^2 \rho (\upsilon^2 - 1)}, \quad J_{10} = -\frac{(3888\pi^4 H^3 E a^2 b^2 + 3240\pi^4 H^3 E b^4)}{75\rho H a^4 b^4 (\upsilon^2 - 1)},$$

$$J_{11} = \frac{\mu}{H\rho}, \quad J_{12} = \frac{4}{25baH\rho},$$

$$J_{13} = -\frac{(40\pi^4 H^3 E b^4 + 48\pi^4 H^3 E a^2 b^2)}{75\rho H a^4 b^4 (\upsilon^2 - 1)}, \quad J_{14} = \frac{96\pi^4 H^2 E}{25 a^2 b^2 \rho (\upsilon^2 - 1)},$$

$$J_{15} = \frac{(4860\pi^4 H^3 E b^4 + 648\pi^4 H^3 E a^2 b^2 + 60\pi^4 H^3 E a^4)}{75\rho H a^4 b^4 (\upsilon^2 - 1)},$$

$$J_{16} = -\frac{(3240\pi^4 H^3 E a^4 + 3888\pi^4 H^3 E a^2 b^2)}{75\rho H a^4 b^4 (\upsilon^2 - 1)}, \quad J_{17} = \frac{\mu}{H\rho}, \quad J_{18} = \frac{4}{25baH\rho},$$

$$J_{19} = \frac{32\pi^4 H^2 E}{75 a^2 b^2 \rho (\upsilon^2 - 1)}, \quad J_{20} = \frac{(-432\pi^4 H^3 E a^2 b^2 - 40\pi^4 H^3 E b^4)}{75\rho H a^4 b^4 (\upsilon^2 - 1)},$$

$$J_{21} = \frac{(-432\pi^4 H^3 E a^2 b^2 - 40\pi^4 H^3 E a^4)}{75\rho H a^4 b^4 (\upsilon^2 - 1)},$$

$$J_{22} = \frac{(4860\pi^4 H^3 E a^4 + 4860\pi^4 H^3 E b^4 + 5832\pi^4 H^3 E a^2 b^2)}{75\rho H a^4 b^4 (\upsilon^2 - 1)},$$

$$J_{23} = \frac{\mu}{H\rho}, \quad J_{24} = \frac{4}{25baH\rho}.$$

APPENDIX E

COMPUTER PROGRAM CODE

The computer program code together with the input and output example are given in the attached CD.